

Long-Chain Alkylthiol Assemblies Containing Buried In-Plane Stabilizing Architectures<sup>†</sup>Hung-Hsun Lee,<sup>‡</sup> Živilė Ruželė,<sup>§</sup> Lyuba Malysheva,<sup>||</sup> Alexander Onipko,<sup>||</sup> Albert Gutés,<sup>‡</sup>  
Fredrik Björefors,<sup>‡</sup> Ramūnas Valiokas,<sup>§</sup> and Bo Liedberg<sup>\*,\*†</sup><sup>‡</sup>Division of Molecular Physics, Department of Physics, Chemistry and Biology, Linköping University, 58183 Linköping, Sweden, <sup>§</sup>Department of Functional Nanomaterials, Institute of Physics, Savanoriu 231, LT-02300 Vilnius, Lithuania, and <sup>||</sup>Bogolyubov Institute for Theoretical Physics, Kiev 03143, Ukraine

Received May 11, 2009. Revised Manuscript Received July 6, 2009

A series of alkylthiol compounds were synthesized to study the formation and structure of complex self-assembled monolayers (SAMs) consisting of interchanging structural modules stabilized by intermolecular hydrogen bonds. The chemical structure of the synthesized compounds, HS(CH<sub>2</sub>)<sub>15</sub>CONH(CH<sub>2</sub>CH<sub>2</sub>O)<sub>6</sub>CH<sub>2</sub>CONH-X, where X refers to the extended chains of either -(CH<sub>2</sub>)<sub>n</sub>CH<sub>3</sub> or -(CD<sub>2</sub>)<sub>n</sub>CD<sub>3</sub>, with *n* = 0, 1, 7, 8, 15, was confirmed by NMR and elemental analysis. The formation of highly ordered, methyl-terminated SAMs on gold from diluted ethanolic solutions of these compounds was revealed using contact angle goniometry, null ellipsometry, cyclic voltammetry, and infrared reflection absorption spectroscopy. The experimental work was complemented with extensive DFT modeling of infrared spectra and molecular orientation. New assignments were introduced for both nondeuterated and deuterated compounds. The latter set of compounds also served as a convenient tool to resolve the packing, conformation, and orientation of the buried and extended modules within the SAM. Thus, it was shown that the lower alkyl portion together with the hexa(ethylene glycol) portion is stabilized by the two layers of lateral hydrogen bonding networks between the amide groups, and they provide a structurally robust support for the extended alkyls. The presented system can be considered to be an extension of the well-known alkyl SAM platform, enabling precise engineering of nanoscopic architectures on the length scale from a few to ~60 Å for applications such as cell membrane mimetics, molecular nanolithography, and so forth.

## 1. Introduction

Self-assembled monolayers (SAMs) of bifunctional compounds on solid surfaces<sup>1,2</sup> today serve as a powerful platform for nanoscience and nanotechnology.<sup>3,4</sup> Among them, SAMs formed by long-chain alkyls with a disulfide or thiol headgroup have become an archetypical system. Since their discovery more than 20 years ago,<sup>5,6</sup> the alkylthiol SAMs have been employed in diverse applications ranging from biosensors and bioarrays to micro- and nanofabrication of electronic devices. The remarkable popularity of this particular system relies on the relative structural simplicity of the constituent compounds, the ease of preparation, and the overall robustness of the obtained SAMs. Normally, the structural characteristics of the alkylthiol SAMs on gold show little sensitivity to factors such as the alkyl chain length and chemical/physical properties of the terminal group. Therefore, their predictable structure and phase behavior offer significant advantages for technological applications. However, many studies have indicated that the introduction of different heteroatoms

or chemical groups along the alkyl chain might have significant structural implications.<sup>7–9</sup> These observations suggest a promising strategy for engineering the structural and functional characteristics of the metal–organic interface. For example, it has been reported that lateral hydrogen bonds formed by buried amide groups affect the electron transfer across the SAM,<sup>10,11</sup> increase the stability of SAMs,<sup>12–14</sup> and promote phase separation into nanoscopic surface domains upon assembly with compounds without the amide group.<sup>15,16</sup> Also, the incorporation of radiation-sensitive groups allows the selective destruction of the SAM, thus creating a platform for micro- and nanofabrication, addressing, and/or in situ synthesis on surfaces.<sup>17</sup> Recently, Allara and co-workers showed that the introduction of an ester moiety into the alkylthiol SAMs causes the formation of a strong dipole layer, thus changing the electrical characteristics of the SAM–gold interphase.<sup>18</sup>

<sup>†</sup> Part of the “Langmuir 25th Year: Self-assembled monolayers: synthesis, characterization, and applications” special issue.

\*Corresponding author. E-mail: bolie@ifm.liu.se. Tel: +46 (0)13 28 18 77. Fax: +46 (0)13 13 75 68.

(1) Ulman, A. *Chem. Rev.* **1996**, *96*, 1533–1554.  
(2) Schreiber, F. *Prog. Surf. Sci.* **2000**, *65*, 151–256.  
(3) Kramer, S.; Fuierer, R. R.; Gorman, C. B. *Chem. Rev.* **2003**, *103*, 4367–4418.  
(4) Love, J. C.; Estroff, L. A.; Kriebel, J. K.; Nuzzo, R. G.; Whitesides, G. M. *Chem. Rev.* **2005**, *105*, 1103–1169.  
(5) Nuzzo, R. G.; Allara, D. L. *J. Am. Chem. Soc.* **1983**, *105*, 4481–4483.  
(6) Porter, M. D.; Bright, T. B.; Allara, D. L.; Chidsey, C. E. D. *J. Am. Chem. Soc.* **1987**, *109*, 3559–3568.  
(7) Evans, S. D.; Goppertberarducci, K. E.; Urankar, E.; Gerenser, L. J.; Ulman, A. *Langmuir* **1991**, *7*, 2700–2709.  
(8) Lenk, T. J.; Hallmark, V. M.; Hoffmann, C. L.; Rabolt, J. F.; Castner, D. G.; Erdelen, C.; Ringsdorf, H. *Langmuir* **1994**, *10*, 4610–4617.

(9) Clegg, R. S.; Reed, S. M.; Smith, R. K.; Barron, B. L.; Rear, J. A.; Hutchison, J. E. *Langmuir* **1999**, *15*, 8876–8883.

(10) Sek, S.; Misicka, A.; Bilewicz, R. *J. Phys. Chem. B* **2000**, *104*, 5399–5402.

(11) Sek, S.; Palys, B.; Bilewicz, R. *J. Phys. Chem. B* **2002**, *106*, 5907–5914.

(12) Tam-Chang, S. W.; Biebuyck, H. A.; Whitesides, G. M.; Jeon, N.; Nuzzo, R. G. *Langmuir* **1995**, *11*, 4371–4382.

(13) Clegg, R. S.; Reed, S. M.; Hutchison, J. E. *J. Am. Chem. Soc.* **1998**, *120*, 2486–2487.

(14) Valiokas, R.; Ostblom, M.; Svedhem, S.; Svensson, S. C. T.; Liedberg, B. *J. Phys. Chem. B* **2002**, *106*, 10401–10409.

(15) Lewis, P. A.; Smith, R. K.; Kelly, K. F.; Bumm, L. A.; Reed, S. M.; Clegg, R. S.; Gunderson, J. D.; Hutchison, J. E.; Weiss, P. S. *J. Phys. Chem. B* **2001**, *105*, 1119–1122.

(16) Smith, R. K.; Reed, S. M.; Lewis, P. A.; Monnell, J. D.; Clegg, R. S.; Kelly, K. F.; Bumm, L. A.; Hutchison, J. E.; Weiss, P. S. *J. Phys. Chem. B* **2001**, *105*, 1119–1122.

(17) Heister, K.; Frey, S.; Ulman, A.; Grunze, M.; Zharnikov, M. *Langmuir* **2004**, *20*, 1222–1227.

(18) Cabarcos, O. M.; Shaporenko, A.; Weidner, T.; Uppili, S.; Dake, L. S.; Zharnikov, M.; Allara, D. L. *J. Phys. Chem. C* **2008**, *112*, 10842–10854.

In the biomaterials and life science communities, SAMs formed by different oligo(ethylene glycol) (OEG) derivatives (most often OEG- and PEG-terminated alkylthiol SAMs) have attracted a lot of attention.<sup>19</sup> They proved to be a reliable strategy for engineering protein- and cell-specific interfaces, at the same time enabling the control of nonspecific protein binding. An interesting structural aspect of this type of SAMs is that for certain oligomer lengths, which depend on the presence/length of the alkyl spacer, the incorporation of other specific chemical groups, and the type of substrate (e.g., gold or silver), the OEG portion adopts a helical conformation.<sup>20</sup> This crystalline OEG phase in the SAMs is distorted by the strong interaction between the oxygen of the OEG and the hydroxyl ions in water.<sup>21</sup> However, when water is absent, the OEG SAMs display remarkable structural uniformity and therefore they can be used as a reference material<sup>22,23</sup> or as a building block to construct sophisticated molecular nanoarchitectures, thus extending the available toolbox of alkylthiol compounds.

Previously, we reported on a so-called “modular approach” to assemble structurally complex SAMs with increased thermal stability by taking advantage of different structural modules. By combining the alkyl, OEG, and amide moieties, Svedhem et al.<sup>24</sup> synthesized a compound, HS(CH<sub>2</sub>)<sub>15</sub>–CONH–(CH<sub>2</sub>CH<sub>2</sub>O)<sub>6</sub>CH<sub>2</sub>–CONH–(CH<sub>2</sub>)<sub>15</sub>–CH<sub>3</sub> which formed highly ordered, 60-Å-thick SAMs on Au(111).<sup>25</sup> This SAM displayed remarkable phase stability up to ~130 °C. Notably, infrared reflection absorption spectroscopy (IRAS) of this SAM revealed that the terminal methyl groups display a specific signature, namely, splitting of the asymmetric methyl C–H stretch, which is otherwise seen only for long-chain alkylthiol SAMs below 200 K.<sup>26</sup> Also, the infrared RA spectrum of these SAMs contained much stronger and sharper bands originating from different modes of the helical OEG segment as compared to OEG SAMs formed by compounds without the extended alkyl chain. Very recently, we presented preliminary ab initio modeling data that indicated that the orientation of the constituent modules of the HS(CH<sub>2</sub>)<sub>15</sub>–CONH–(CH<sub>2</sub>CH<sub>2</sub>O)<sub>6</sub>CH<sub>2</sub>–CONH–(CH<sub>2</sub>)<sub>15</sub>–CH<sub>3</sub> compound may significantly differ as compared to less complex alkyl thiol SAMs consisting of shorter alkyl and/or OEG portions.<sup>27</sup>

The above-mentioned structural peculiarities encouraged us to undertake a systematic investigation of the role of the individual modules in such structurally complex SAMs as HS(CH<sub>2</sub>)<sub>15</sub>–CONH–(CH<sub>2</sub>CH<sub>2</sub>O)<sub>6</sub>CH<sub>2</sub>–CONH–(CH<sub>2</sub>)<sub>15</sub>–CH<sub>3</sub>. Here we report on the synthesis, characterization, and theoretical modeling of SAMs formed by a series of structurally self-consistent compounds (Scheme 1). These compounds were synthesized to reveal the role of an additional amide and the length of the extended alkyl chain on the structural and blocking characteristics. The SAMs were also characterized by employing

contact angle goniometry, ellipsometry, electrochemistry, and IRAS. Moreover, we used a set of ab initio–DFT approaches, which previously have been optimized to explore the infrared signatures of OEG-terminated SAMs,<sup>28–32</sup> a powerful tool to reveal the possible orientation and packing of the different moieties of the SAM-forming compounds on gold. The present study demonstrates that the incorporation of complex in-plane stabilizing architectures such as amide and OEG moieties extends the possibility to obtain highly ordered, electrically isolating SAMs in the thickness range of at least up to 60 Å. We anticipate that such a novel SAM platform will be of interest in materials science and technology. For example, nanopatterns consisting of SAMs with variable extended alkyl chains can be employed as supports for the assembly of artificial cell membranes for incorporation, analysis, and manipulation of membrane proteins. The synthesis of similar compounds with functional terminal groups could also be explored. Moreover, the structural uniformity and robustness of these SAMs as well as different sensitivity of the interchanging modules to external factors such as temperature or radiation may provide interesting approaches for materials engineering beyond biological applications.

## 2. Materials and Methods

**2.1. Synthesis.** All reagents were obtained from commercial suppliers and were used without further purification. NMR spectra were recorded on a Varion INOVA spectrometer (300 MHz). Elemental analyses were carried out by Analytische Laboratorien, Lindlar, Germany. H and D were calculated as H (measured by TCD) for the deuterated compounds. The synthesis of the reference compound (bottom Scheme 1) is described elsewhere.<sup>24</sup>

**2.1.1. General Procedure for Amine Coupling and Subsequent Deprotection of Acetylated Thiols.** To a solution of compound **1**<sup>24</sup> (1 equiv) in CH<sub>2</sub>Cl<sub>2</sub> or DMF at 0 °C were added amine (1.5 equiv), *N*-hydroxybenzotriazole (HOBt) (1.5 equiv), and *N*-(3-dimethylaminopropyl)-*N*-ethylcarbodiimide (EDC) (1.5 equiv). The reaction mixture was allowed to attain room temperature. After 12–24 h, it was diluted with CH<sub>2</sub>Cl<sub>2</sub> and washed with 0.1 M HCl and water. The organic solution was dried over MgSO<sub>4</sub> and evaporated. Purification was performed by column chromatography (CH<sub>2</sub>Cl<sub>2</sub>/MeOH).

**2.1.2. Deprotection.** A solution of the thioacetate in dry methanol was purged with argon, followed by the addition of acetyl chloride (7.1 μL/mL). The mixture was refluxed under an atmosphere of argon for 5 to 6 h and then cooled to room temperature. Methanol was evaporated and repeatedly coevaporated with dry toluene. Purification was performed by column chromatography (CH<sub>2</sub>Cl<sub>2</sub>/MeOH).

**2.1.3. *N*-[18-(*N*-Methylcarbonyl)methyl-3,6,9,12,15,18-hexaoxaoctadecyl] 16-(Acetylthio)hexadecanamide (**2a**)** [AcS-(CH<sub>2</sub>)<sub>15</sub>CONH(CH<sub>2</sub>CH<sub>2</sub>O)<sub>6</sub>CH<sub>2</sub>CONHMe]. Compound **1** was dissolved in DMF and coupled to methylamine hydrochloride in the presence of triethylamine following the general procedure for amine coupling described above. Yield: 95%. Analytical data: Calcd for C<sub>33</sub>H<sub>64</sub>N<sub>2</sub>O<sub>9</sub>S: C 59.61%, H 9.70%, N 4.21%. Found: C 59.44%, H 9.47%, N 4.01%.

**2.1.4. *N*-[18-(*N*-Methylcarbonyl)methyl-3,6,9,12,15,18-hexaoxaoctadecyl] 16-Mercaptohexadecanamide (**3a**)**

(28) Malysheva, L.; Klymenko, Y.; Onipko, A.; Valiokas, R.; Liedberg, B. *Chem. Phys. Lett.* **2003**, *370*, 451–459.

(29) Malysheva, L.; Onipko, A.; Valiokas, R.; Liedberg, B. *J. Phys. Chem. A* **2005**, *109*, 7788–7796.

(30) Malysheva, L.; Onipko, A.; Valiokas, R.; Liedberg, B. *J. Phys. Chem. B* **2005**, *109*, 13221–13227.

(31) Malysheva, L.; Onipko, A.; Liedberg, B. *J. Phys. Chem. A* **2008**, *112*, 1683–1687.

(32) Malysheva, L.; Onipko, A.; Liedberg, B. *J. Phys. Chem. A* **2008**, *112*, 728–736.

(19) Pale-Grosdemange, C.; Simon, E. S.; Prime, K. L.; Whitesides, G. M. *J. Am. Chem. Soc.* **1991**, *113*, 12–20.

(20) Harder, P.; Grunze, M.; Dahint, R.; Whitesides, G. M.; Laibinis, P. E. *J. Phys. Chem. B* **1998**, *102*, 426–436.

(21) Zolk, M.; Eisert, F.; Pipper, J.; Herrwerth, S.; Eck, W.; Buck, M.; Grunze, M. *Langmuir* **2000**, *16*, 5849–5852.

(22) Vanderah, D. J.; Gates, R. S.; Silin, V.; Zeiger, D. N.; Woodward, J. T.; Meuse, C. W.; Valincius, G.; Nickel, B. *Langmuir* **2003**, *19*, 2612–2620.

(23) Vanderah, D. J.; Parr, T.; Silin, V.; Meuse, C. W.; Gates, R. S.; La, H. Y.; Valincius, G. *Langmuir* **2004**, *20*, 1311–1316.

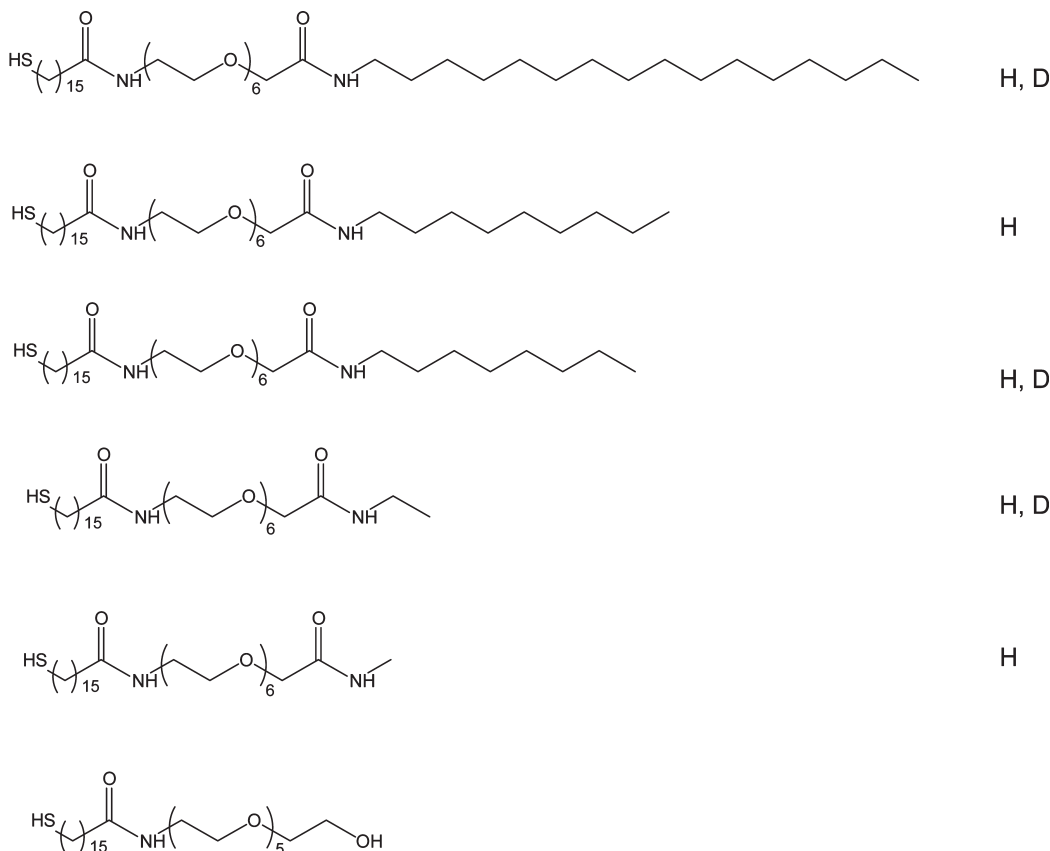
(24) Svedhem, S.; Hollander, C. A.; Shi, J.; Konradsson, P.; Liedberg, B.; Svensson, S. C. T. *J. Org. Chem.* **2001**, *66*, 4494–4503.

(25) Valiokas, R.; Ostblom, M.; Bjorefors, F.; Liedberg, B.; Shi, J.; Konradsson, P. *Biointerphases* **2006**, *1*, 22–34.

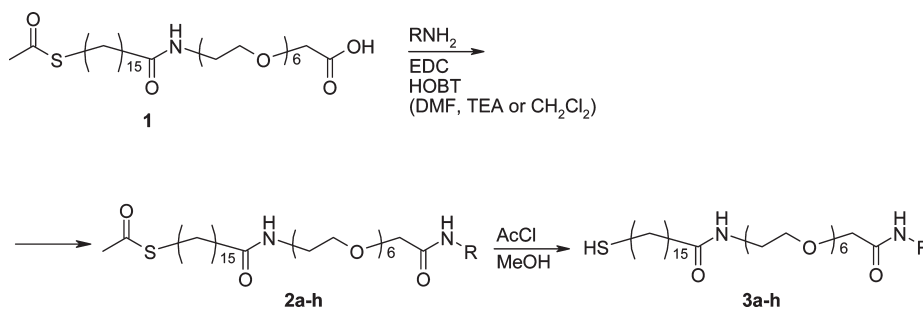
(26) Nuzzo, R. G.; Korenic, E. M.; Dubois, L. H. *J. Chem. Phys.* **1990**, *93*, 767–773.

(27) Valiokas, R.; Malysheva, L.; Onipko, A.; Lee, H.-H.; Ruzel, Z.; Svedhem, S.; Svensson, S. C. T.; Gelius, U.; Liedberg, B. *J. Electron Spectrosc. Relat. Phenom.*, in press.

**Scheme 1. Investigated Compounds with Deuterated (D) and Nondeuterated (H) Extended Chains and the Reference Compound without an Extended Alkyl Chain**



**Scheme 2. Synthesis of Alkyl-Terminated OEG Thiol Compounds (3a–h)<sup>a</sup>**



<sup>a</sup> Abbreviations: RNH<sub>2</sub>, methylamine (a), ethylamine hydrochloride (b), ethyl-*d*<sub>5</sub>-amine hydrochloride (c), *n*-octylamine (d), *n*-octyl-*d*<sub>17</sub>-amine (e), *n*-nonylamine (f), *n*-hexadecylamine (g), *n*-hexadecyl-*d*<sub>33</sub>-amine (h); EDC, *N*-(3-dimethylaminopropyl)-*N*-ethylcarbodiimide; HOBT, *N*-hydroxybenzotriazole; DMF, *N,N*-dimethylformamide; TEA, triethylamine; AcCl, acetylchloride.

[HS(CH<sub>2</sub>)<sub>15</sub>CONH(CH<sub>2</sub>CH<sub>2</sub>O)<sub>6</sub>CH<sub>2</sub>CONHMe]. <sup>1</sup>H NMR (CDCl<sub>3</sub>) δ 7.10 (s, 1H), 6.18 (t, 1H), 3.98 (s, 2H), 3.65–3.59 (m, 20H), 3.55–3.52 (m, 2H), 3.45–3.42 (m, 2H), 2.83 (d, 3H), 2.51 (q, 2H), 2.16 (t, 2H), 2.05 (s, 1H), 1.63–1.57 (m, 4H), 1.36–1.24 (m, 22H). Analytical data: Calcd for C<sub>31</sub>H<sub>62</sub>N<sub>2</sub>O<sub>8</sub>S: C 59.77%, H 10.03%, N 4.50%. Found: C 59.56%, H 10.01%, N 4.39%.

2.1.5. *N*-[18-(*N*-Ethylcarbamoyl)methyl-3,6,9,12,15,18-hexaoxaoctadecyl] 16-(Acetylthio)hexadecanamide (**2b**) [AcS(CH<sub>2</sub>)<sub>15</sub>CONH(CH<sub>2</sub>CH<sub>2</sub>O)<sub>6</sub>CH<sub>2</sub>CONHEt]. Compound **1** was dissolved in DMF and coupled to ethylamine hydrochloride in the presence of triethylamine following the general procedure for the amine coupling described above. Yield: 90%. Analytical data: Calcd for C<sub>34</sub>H<sub>66</sub>N<sub>2</sub>O<sub>9</sub>S: C 60.15%, H 9.80%, N 4.13%. Found: C 60.18%, H 9.91%, N 4.09%.

2.1.6. *N*-[18-(*N*-Ethylcarbamoyl)methyl-3,6,9,12,15,18-hexaoxaoctadecyl] 16-Mercaptohexadecanamide (**3b**) [HS(CH<sub>2</sub>)<sub>15</sub>CONH(CH<sub>2</sub>CH<sub>2</sub>O)<sub>6</sub>CH<sub>2</sub>CONHEt]. <sup>1</sup>H NMR (CDCl<sub>3</sub>) δ 6.98

(s, 1H), 6.15 (t, 1H), 3.96 (s, 2H), 3.65–3.59 (m, 20H), 3.55–3.52 (m, 2H), 3.45–3.41 (m, 2H), 3.35–3.29 (m, 2H), 2.50 (q, 2H), 2.15 (t, 2H), 1.62–1.52 (m, 5H), 1.36–1.24 (m, 23H), 1.15 (t, 2H). <sup>13</sup>C NMR (CDCl<sub>3</sub>) δ 173.3, 169.8, 71.0, 70.7, 70.6, 70.5, 70.4, 70.3, 70.1, 39.2, 36.8, 34.1, 33.7, 29.7, 29.65, 29.6, 29.5, 29.4, 29.1, 28.4, 25.8, 24.7, 14.9. Analytical data: Calcd for C<sub>32</sub>H<sub>64</sub>N<sub>2</sub>O<sub>8</sub>S: C 60.34%, H 10.13%, N 4.40%. Found: C 60.18%, H 10.06%, N 4.22%.

2.1.7. *N*-[18-(*N*-Ethyl-*d*<sub>5</sub>-carbamoyl)methyl-3,6,9,12,15,18-hexaoxaoctadecyl] 16-(Acetylthio)hexadecanamide (**2c**) [AcS(CH<sub>2</sub>)<sub>15</sub>CONH(CH<sub>2</sub>CH<sub>2</sub>O)<sub>6</sub>CH<sub>2</sub>CONHCD<sub>2</sub>CD<sub>3</sub>]. Compound **1** was dissolved in DMF and coupled to ethyl-*d*<sub>5</sub>-amine hydrochloride in the presence of triethylamine following the general procedure for amine coupling described above. Yield: 90%. Analytical data: Calcd for C<sub>40</sub>H<sub>78</sub>N<sub>2</sub>O<sub>9</sub>S: C 62.96%, H 10.30%, N 3.67%. Found: C 62.99%, H 10.30%, N 3.60%.

2.1.8. *N*-[18-(*N*-Ethyl-*d*<sub>5</sub>-carbamoyl)methyl-3,6,9,12,15,18-hexaoxaoctadecyl] 16-Mercaptohexadecanamide (**3c**)

[ $HS(CH_2)_{15}CONH(CH_2CH_2O)_6CH_2CONHCD_2CD_3$ ].  $^1H$  NMR ( $CDCl_3$ )  $\delta$  6.97 (s, 1H), 6.08 (s, 1H), 3.97 (s, 2H), 3.68–3.60 (m, 20H), 3.57–3.53 (m, 2H), 3.50–3.42 (m, 2H), 2.52 (q, 2H), 2.16 (t, 2H), 1.66–1.57 (m, 5H), 1.36–1.25 (m, 22H).  $^{13}C$  NMR ( $CDCl_3$ )  $\delta$  173.3, 169.8, 71.1, 70.75, 70.7, 70.65, 70.6, 70.4, 70.3, 70.1, 39.3, 36.9, 34.2, 29.8, 29.7, 29.6, 29.55, 29.5, 29.2, 28.5, 25.9, 24.8. Analytical data: Calcd for  $C_{32}H_{59}D_5N_2O_8S$ : C 59.87%, (H + D calcd as H) 10.21%, N 4.36%. Found: C 59.66%, (H + D) 9.96%, N 4.24%.

2.1.9. *N*-[18-(*N*-Octylcarbamoyl)methyl-3,6,9,12,15,18-hexaoxaoctadecyl] 16-(Acetylthio)hexadecanamide (**2d**) [ $AcS(CH_2)_{15}CONH(CH_2CH_2O)_6CH_2CONH(CH_2)_7CH_3$ ]. Compound **1** was dissolved in  $CH_2Cl_2$  and coupled to *n*-octylamine following the general procedure for amine coupling described above. Yield: 89%. Analytical data: Calcd for  $C_{40}H_{78}N_2O_9S$ : C 62.96%, H 10.30%, N 3.67%. Found: C 62.99%, H 10.30%, N 3.60%.

2.1.10. *N*-[18-(*N*-Octylcarbamoyl)methyl-3,6,9,12,15,18-hexaoxaoctadecyl] 16-Mercaptohexadecanamide (**3d**) [ $HS(CH_2)_{15}CONH(CH_2CH_2O)_6CH_2CONH(CH_2)_7CH_3$ ].  $^1H$  NMR ( $CDCl_3$ )  $\delta$  6.91 (s, 1H), 6.08 (t, 1H), 3.97 (s, 2H), 3.67–3.59 (m, 20H), 3.56–3.52 (m, 2H), 3.46–3.41 (m, 2H), 3.27 (q, 2H), 2.51 (q, 2H), 2.16 (t, 2H), 1.71 (s, 1H), 1.65–1.48 (m, 6H), 1.37–1.25 (m, 32H), 0.87 (t, 3H).  $^{13}C$  NMR ( $CDCl_3$ )  $\delta$  173.4, 169.9, 71.1, 70.8, 70.75, 70.7, 70.6, 70.5, 70.4, 70.2, 39.3, 39.1, 36.9, 34.2, 32.0, 29.8, 29.75, 29.7, 29.6, 29.5, 29.45, 29.4, 29.2, 28.5, 27.1, 25.9, 24.8, 22.8, 14.2. Analytical data: Calcd for  $C_{38}H_{76}N_2O_8S$ : C 63.29%, H 10.62%, N 3.88%. Found: C 63.15%, H 10.59%, N 3.83%.

2.1.11. *N*-[18-(*N*-Octyl- $d_{17}$ -carbamoyl)methyl-3,6,9,12,15,18-hexaoxaoctadecyl] 16-(Acetylthio)hexadecanamide (**2e**) [ $AcS(CH_2)_{15}CONH(CH_2CH_2O)_6CH_2CONH(CD_2)_7CD_3$ ]. Compound **1** was dissolved in  $CH_2Cl_2$  and coupled to *n*-octyl- $d_{17}$ -amine following the general procedure for amine coupling described above. Yield: 96%. Analytical data: Calcd for  $C_{40}H_{61}D_{17}N_2O_9S$ : C 61.58%, (H + D calcd as H) 10.53%, N 3.59%. Found: C 61.57%, (H + D) 10.21%, N 3.52%.

2.1.12. *N*-[18-(*N*-Octyl- $d_{17}$ -carbamoyl)methyl-3,6,9,12,15,18-hexaoxaoctadecyl] 16-Mercaptohexadecanamide (**3e**) [ $HS(CH_2)_{15}CONH(CH_2CH_2O)_6CH_2CONH(CD_2)_7CD_3$ ].  $^1H$  NMR ( $CDCl_3$ )  $\delta$  6.91 (s, 1H), 6.09 (t, 1H), 3.97 (s, 2H), 3.66–3.60 (m, 20H), 3.56–3.53 (m, 2H), 3.47–3.40 (m, 2H), 2.51 (q, 2H), 2.16 (t, 2H), 1.78 (s, 1H), 1.70–1.50 (m, 4H), 1.40–1.24 (m, 22H).  $^{13}C$  NMR ( $CDCl_3$ )  $\delta$  173.4, 169.9, 71.1, 70.85, 70.8, 70.75, 70.7, 70.5, 70.4, 70.2, 39.3, 36.9, 34.2, 29.85, 29.8, 29.7, 29.6, 29.5, 29.2, 28.5, 25.9, 24.8. Analytical data: Calcd for  $C_{38}H_{59}D_{17}N_2O_8S$ : C 61.83%, (H + D calcd as H) 10.87%, N 3.79%. Found: C 61.57%, (H + D) 10.38%, N 3.62%.

2.1.13. *N*-[18-(*N*-Nonylcarbamoyl)methyl-3,6,9,12,15,18-hexaoxaoctadecyl] 16-(Acetylthio)hexadecanamide (**2f**) [ $AcS(CH_2)_{15}CONH(CH_2CH_2O)_6CH_2CONH(CH_2)_8CH_3$ ]. Compound **1** was dissolved in  $CH_2Cl_2$  and coupled to *n*-nonylamine following the general procedure for amine coupling described above. Yield: 54%. Analytical data: Calcd for  $C_{41}H_{80}N_2O_9S$ : C 63.36%, H 10.38%, N 3.60%. Found: C 63.21%, H 10.41%, N 3.74%.

2.1.14. *N*-[18-(*N*-Nonylcarbamoyl)methyl-3,6,9,12,15,18-hexaoxaoctadecyl] 16-Mercaptohexadecanamide (**3f**) [ $HS(CH_2)_{15}CONH(CH_2CH_2O)_6CH_2CONH(CH_2)_8CH_3$ ].  $^1H$  NMR ( $CDCl_3$ )  $\delta$  6.90 (t, 1H), 6.05 (t, 1H), 3.96 (s, 2H), 3.65–3.60 (m, 20H), 3.55–3.52 (m, 2H), 3.45–3.41 (m, 2H), 3.26 (q, 2H), 2.51 (q, 2H), 2.15 (t, 2H), 1.98 (s, 1H), 1.62–1.47 (m, 6H), 1.36–1.24 (m, 34H), 0.86 (t, 3H).  $^{13}C$  NMR ( $CDCl_3$ )  $\delta$  173.5, 169.9, 71.2, 70.9, 70.85, 70.8, 70.7, 70.5, 70.4, 70.2, 39.4, 39.1, 36.9, 34.3, 32.1, 29.9, 29.8, 29.75, 29.7, 29.65, 29.6, 29.5, 29.3, 28.6, 27.2, 26.0, 24.9, 22.9, 14.3. Analytical data: Calcd for  $C_{39}H_{78}N_2O_8S$ : C 63.72%, H 10.69%, N 3.81%. Found: C 63.02%, H 10.48%, N 3.66%.

2.1.15. *N*-[18-(*N*-Hexadecylcarbamoyl)methyl-3,6,9,12,15,18-hexaoxaoctadecyl] 16-Mercaptohexadecanamide (**3g**)

[ $HS(CH_2)_{15}CONH(CH_2CH_2O)_6CH_2CONH(CH_2)_{15}CH_3$ ]. This compound was synthesized following the protocol by Svedhem,<sup>24</sup> and an identical structure was confirmed by NMR.

2.1.16. *N*-[18-(*N*-Hexadecyl- $d_{33}$ -carbamoyl)methyl-3,6,9,12,15,18-hexaoxaoctadecyl] 16-(Acetylthio)hexadecanamide (**2h**) [ $AcS(CH_2)_{15}CONH(CH_2CH_2O)_6CH_2CONH(CD_2)_{15}CD_3$ ]. Compound **1** was dissolved in  $CH_2Cl_2$  and coupled to *n*-hexadecyl- $d_{33}$ -amine following the general procedure for amine coupling described above. Yield: 95%. Analytical data: Calcd for  $C_{46}H_{59}D_{33}N_2O_8S$ : C 63.47%, (H + D calcd as H) 11.22%, N 3.08%. Found: C 63.28%, (H + D) 10.81%, N 2.98%.

2.1.17. *N*-[18-(*N*-Hexadecyl- $d_{33}$ -carbamoyl)methyl-3,6,9,12,15,18-hexaoxaoctadecyl] 16-Mercaptohexadecanamide (**3h**) [ $HS(CH_2)_{15}CONH(CH_2CH_2O)_6CH_2CONH(CD_2)_{15}CD_3$ ].  $^1H$  NMR ( $CDCl_3$ )  $\delta$  6.90 (s, 1H), 6.08 (t, 1H), 3.97 (s, 2H), 3.66–3.60 (m, 20H), 3.56–3.53 (m, 2H), 3.47–3.40 (m, 2H), 2.51 (q, 2H), 2.16 (t, 2H), 1.73 (s, 1H), 1.64–1.56 (m, 4H), 1.39–1.25 (m, 22H).  $^{13}C$  NMR ( $CDCl_3$ )  $\delta$  173.3, 169.8, 71.0, 70.75, 70.7, 70.65, 70.6, 70.4, 70.3, 70.1, 39.2, 36.8, 34.1, 29.75, 29.7, 29.6, 29.5, 29.4, 29.1, 28.4, 25.8, 24.7. Analytical data: Calcd for  $C_{46}H_{59}D_{33}N_2O_8S$ : C 63.77%, (H + D calcd as H) 11.57%, N 3.23%. Found: C 62.49%, (H + D) 10.73%, N 3.04%.

**2.2. Self-Assembled Monolayer (SAM) Preparation.** Solutions of the thiols (20  $\mu$ M) in ethanol (99.5%) were prepared in plastic beakers from 1 mM stock solutions and stored in glass vials at room temperature. A 25 Å titanium adhesion layer with an additional 2000-Å-thick gold film was electron beam deposited on standard silicon (100) wafers and used as a substrate for the SAMs. The electron beam evaporation of the metals was performed by employing a Balzers UMS 500 P system operating at a base pressure of  $10^{-9}$  mbar and at an evaporation pressure of about  $10^{-7}$  mbar. A constant evaporation rate of 10 Å/s was used for the gold layer. The resulting polycrystalline gold film was heavily dominated by (111) texture. Prior to SAM adsorption, the gold surfaces were cleaned in a 5:1:1 mixture of deionized water (Milli-Q), 25% hydrogen peroxide, and 30% ammonia for 5 min at 80 °C and then rinsed in deionized water. To check the efficiency of cleaning, the optical characteristics of a gold surface that was taken from the cleaned batch were measured before incubation of the SAMs. The rest of the cleaned gold surfaces were soaked in ethanol and then transferred into the incubation solutions. After at least 48 h of adsorption, the samples were rinsed in ethanol, ultrasonicated for 5 min, and rinsed again. Finally, they were dried in a flow of nitrogen gas and immediately analyzed.

**2.3. Ellipsometry.** Null ellipsometry using a He–Ne laser light source,  $\lambda = 632.8$  nm, at an angle of incidence of 70° was used to determine the thicknesses of the SAMs by means of automatic Rudolph Research AutoEL ellipsometer software. Before SAM preparation, the refractive index of a cleaned gold surface was measured. The obtained average value of the refractive index was later used in an ambient/organic film/gold model assuming an isotropic, transparent organic layer with a refractive index of  $n = 1.5$ . The film thickness was calculated as an average of measurements at three different spots for at least three samples for each compound.

**2.4. Contact Angle Goniometry.** A semiautomatic optical contact angle meter (KSV CAM 200) was used to determine advancing and receding contact angles of water on the SAMs. A manual dispenser was used to expand or retract a droplet. As the drop was dispensed onto the surface and expanded, the advancing contact angle was measured quasi-statically. Similarly, the receding contact angle was measured by partially withdrawing the drop back into the syringe. During the measurements, the syringe needle was kept inside the center of the drop, and a high-speed CCD camera was used for image capturing. The images were analyzed by KSV CAM software. The data shown in this article are averages of three samples. Two to three measurements

were made on each sample, and each measurement consisted of three to five images for the advancing and receding angles, respectively.

**2.5. Electrochemistry.** An Autolab PGSTAT20 (Eco-Chemie, The Netherlands) was used for the voltammetric experiments. All experiments were performed in three-electrode mode using an Ag/AgCl reference electrode (RE-5B, BAS) and a platinum wire as a counter electrode. SAM-coated gold surfaces were brought into contact with the electrolyte via press fitting to an O-ring on the side of a Kel-F-based electrochemical cell. The exposed area of the electrode was 0.20 cm<sup>2</sup>. Cyclic voltammograms were recorded by scanning the potential from 0.40 to -0.30 V (vs Ag/AgCl) and back at a scan rate of 10 mV/s. To provide redox species, a 1.0 mM K<sub>3</sub>Fe(CN)<sub>6</sub> (Merck) solution was used (also containing 100 mM KNO<sub>3</sub> (Merck) as the supporting electrolyte). The nonfaradaic background current was recorded by scanning the potential in only the supporting electrolyte.

**2.6. Infrared Reflection Absorption Spectroscopy.** The reflection-absorption (RA) spectra were recorded on a Bruker IFS 66 system equipped with a grazing angle (85°) infrared reflection accessory and a liquid-nitrogen-cooled MCT detector. The sample chamber was continuously purged with nitrogen gas during the measurement. All spectra were acquired at 2 cm<sup>-1</sup> resolution between 4000 and 700 cm<sup>-1</sup> as the sum of 3000 scans. A three-term Blackmann-Harris apodization function was applied to the interferograms before Fourier transformation. Background spectra (*R*<sub>0</sub>) were taken using a deuterated hexadecanethiol (HS(CD<sub>2</sub>)<sub>15</sub>CD<sub>3</sub>) SAM or a nondeuterated hexadecanethiol (HS(CH<sub>2</sub>)<sub>15</sub>CH<sub>3</sub>) SAM on gold, depending on the spectral range of interest. The sample spectra (*R*) were acquired under identical conditions.

**2.7. Quantum Chemical Calculations.** All calculations were performed by the DFT methods, as provided by the Gaussian 03 package of programs. To find optimized geometries, vibrational frequencies, and transition dipole moments (TDMs) for the molecules listed in Table 1, the BP86 exchange-correlation functional (a GGA functional combining the Becke 88 exchange and Perdew 86 correlation functional) with a 6-31G\* basis set was used. The largest analyzed molecule, EG<sub>6</sub>AC<sub>16</sub>H (Table 1), has 149 atoms with 462 electrons (1043 basis functions), as compared to 66 atoms with 200 electrons (574 basis functions) in recent all-electron ab initio calculations.<sup>18</sup> The TDMs were recalculated for the system of coordinates of the lower alkyl chain. The model spectra were obtained as the sum of Lorentzian-shaped peaks, each centered at the fundamental mode frequency. For part of the modeling, the calculations were duplicated with the Becke's three-parameter hybrid correlation functional (B3LYP) and the Perdew-Burke-Ernzerhof (PBE) functional. The overall comparison of model results with experimental data favors the use of the BP86 method.

### 3. Results

#### 3.1. Ellipsometry and Contact Angle Measurements.

Null ellipsometry and water contact angle measurements were used to characterize SAMs in terms of molecular packing and wetting characteristics. For simplicity, a list of the investigated molecules and their SAM abbreviations is given in Table 1. Table 2 summarizes the measured contact angles and the thicknesses obtained experimentally and from DFT calculations. The measured thicknesses of the investigated SAMs agree well with the DFT-calculated molecular lengths and expected orientation adopted by molecules within the SAMs. The calculations have been performed for two possible attachments of the upper alkyl to the amide nitrogen: conformer I with a negative and conformer II with a positive dihedral angle  $\tau$ (CNCC) that give very similar thicknesses as shown in Table 2. The contact angles for the SAMs generated from the longer compounds (EG<sub>6</sub>AC<sub>8</sub>H, EG<sub>6</sub>AC<sub>9</sub>H,

**Table 1. List of Investigated Compounds and Their SAM Abbreviations<sup>a</sup>**

synthesized compounds	abbreviations
HS(CH <sub>2</sub> ) <sub>15</sub> CONH(CH <sub>2</sub> CH <sub>2</sub> O) <sub>6</sub> CH <sub>2</sub> CONH-(CH <sub>2</sub> ) <sub>15</sub> CH <sub>3</sub> ; <b>3g</b>	EG <sub>6</sub> AC <sub>16</sub> H
HS(CH <sub>2</sub> ) <sub>15</sub> CONH(CH <sub>2</sub> CH <sub>2</sub> O) <sub>6</sub> CH <sub>2</sub> CONH-(CH <sub>2</sub> ) <sub>8</sub> CH <sub>3</sub> ; <b>3f</b>	EG <sub>6</sub> AC <sub>9</sub> H
HS(CH <sub>2</sub> ) <sub>15</sub> CONH(CH <sub>2</sub> CH <sub>2</sub> O) <sub>6</sub> CH <sub>2</sub> CONH-(CH <sub>2</sub> ) <sub>7</sub> CH <sub>3</sub> ; <b>3d</b>	EG <sub>6</sub> AC <sub>8</sub> H
HS(CH <sub>2</sub> ) <sub>15</sub> CONH(CH <sub>2</sub> CH <sub>2</sub> O) <sub>6</sub> CH <sub>2</sub> CONH-(CH <sub>2</sub> )CH <sub>3</sub> ; <b>3b</b>	EG <sub>6</sub> AC <sub>2</sub> H
HS(CH <sub>2</sub> ) <sub>15</sub> CONH(CH <sub>2</sub> CH <sub>2</sub> O) <sub>6</sub> CH <sub>2</sub> CONH-CH <sub>3</sub> ; <b>3a</b>	EG <sub>6</sub> AC <sub>1</sub> H
HS(CH <sub>2</sub> ) <sub>15</sub> CONH(CH <sub>2</sub> CH <sub>2</sub> O) <sub>6</sub> CH <sub>2</sub> CONH-(CD <sub>2</sub> ) <sub>15</sub> CD <sub>3</sub> ; <b>3h</b>	EG <sub>6</sub> AC <sub>16</sub> D
HS(CH <sub>2</sub> ) <sub>15</sub> CONH(CH <sub>2</sub> CH <sub>2</sub> O) <sub>6</sub> CH <sub>2</sub> CONH-(CD <sub>2</sub> ) <sub>7</sub> CD <sub>3</sub> ; <b>3e</b>	EG <sub>6</sub> AC <sub>8</sub> D
HS(CH <sub>2</sub> ) <sub>15</sub> CONH(CH <sub>2</sub> CH <sub>2</sub> O) <sub>6</sub> CH <sub>2</sub> CONH-(CD <sub>2</sub> )CD <sub>3</sub> ; <b>3c</b>	EG <sub>6</sub> AC <sub>2</sub> D
HS(CH <sub>2</sub> ) <sub>15</sub> CONH(CH <sub>2</sub> CH <sub>2</sub> O) <sub>6</sub> -H	EG <sub>6</sub> H

<sup>a</sup>The incorporation of a CH<sub>2</sub> group attached to the upper amide is referred to as A. Hydrogen H and deuterium D denote the versions of the extended chains, -(CH<sub>2</sub>)<sub>n</sub>CH<sub>3</sub> or -(CD<sub>2</sub>)<sub>n</sub>CD<sub>3</sub>, where *n* = 0, 1, 7, 8, 15. The number in bold refers to the abbreviations used in section 2.1.

**Table 2. Ellipsometric thickness *d* and advancing ( $\theta_a$ ) and receding ( $\theta_r$ ) water contact angles of the extended-chain alkylthiol SAMs on gold<sup>a</sup>**

SAM	exp <i>d</i> [Å]	calcd <i>d</i> [Å], conf I/II	$\theta_a$ [deg] ± 1	$\theta_r$ [deg] ± 1
EG <sub>6</sub> AC <sub>16</sub> H	59.0 ± 0.2	59.6/59.9	112	107
EG <sub>6</sub> AC <sub>9</sub> H	50.7 ± 0.6	51.8/53.6	111	106
EG <sub>6</sub> AC <sub>8</sub> H	49.9 ± 0.3	50.1/51.8	111	106
EG <sub>6</sub> AC <sub>2</sub> H	43.0 ± 0.8	43.7/44.9	90	80
EG <sub>6</sub> AC <sub>1</sub> H	41.8 ± 0.5	43.4	66	57
EG <sub>6</sub> H	38.0 ± 0.5	39.7	30	25
EG <sub>6</sub> AC <sub>16</sub> D	58.6 ± 0.4	59.6/59.9	112	107
EG <sub>6</sub> AC <sub>8</sub> D	49.4 ± 0.3	50.1/51.8	112	106
EG <sub>6</sub> AC <sub>2</sub> D	42.1 ± 0.3	43.7/44.9	92	83

<sup>a</sup>Calculated thicknesses are represented for two molecular conformers I/II. See section 3.4 for details.

EG<sub>6</sub>AC<sub>16</sub>H), both deuterated and nondeuterated, are essentially identical with advancing and receding contact angle values around 112 and 107°, respectively. These values and the low hysteresis of 5° are indicative of chemically and structurally homogeneous SAMs possessing densely packed and highly oriented methylene chains with the methyl exposed to the ambient atmosphere. However, the SAMs having shorter alkyl chains display considerably lower contact angle values and a higher hysteresis, most likely because of the increasing exposure of the underlying groups in the SAMs to the contacting liquid. For example, the substantial lowering in contact angles seen for the three shortest compounds EG<sub>6</sub>AC<sub>1</sub>H, EG<sub>6</sub>AC<sub>2</sub>H, and EG<sub>6</sub>AC<sub>2</sub>D, and EG<sub>6</sub>AC<sub>1</sub>H in particular, can be attributed to the different contribution from the polar amide group, which for the above SAMs appears within the "sensing depth" of the contacting liquid, ~5 Å for water.<sup>33</sup> Furthermore, the contact angles showed no odd-even number dependence for EG<sub>6</sub>AC<sub>8</sub>H and EG<sub>6</sub>AC<sub>9</sub>H SAMs. To summarize, the ellipsometric thickness and contact angle data suggest that the investigated compounds with an extended chain of *n* ≥ 7 form densely packed, well-oriented SAMs. The alkyl chain conformation of the SAMs will be discussed further in section 3.3.1.

**3.2. Blocking Characteristics.** Cyclic voltammetry (CV) provides information on the blocking characteristics of organic

(33) Bain, C. D.; Whitesides, G. M. *J. Am. Chem. Soc.* **1988**, *110*, 5897-5898.

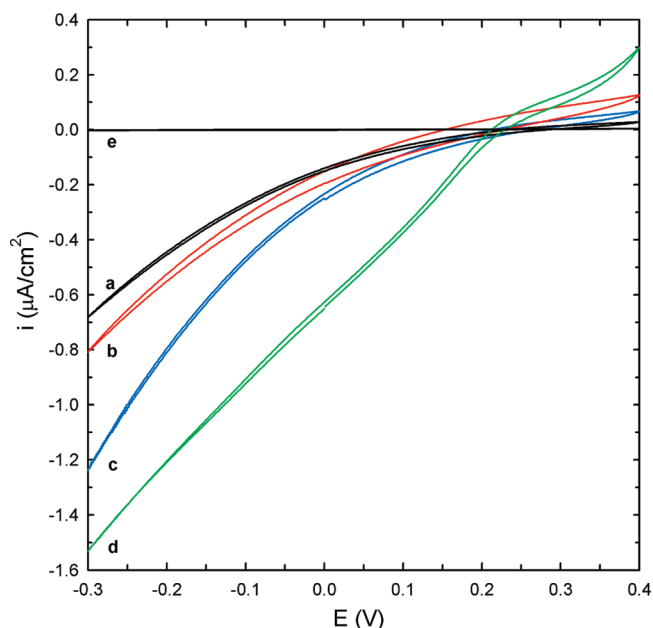


**Figure 1.** Cyclic voltammograms of the three different SAMs EG<sub>6</sub>AC<sub>16</sub>H (a), EG<sub>6</sub>AC<sub>8</sub>H (b), and EG<sub>6</sub>AC<sub>2</sub>H (c) and hexadecanethiol (d) obtained in a 1.0 mM K<sub>3</sub>Fe(CN)<sub>6</sub> aqueous solution (also containing 100 mM KNO<sub>3</sub>). The line close to zero current (e) is the CV of the hexadecanethiol SAM in only the supporting electrolyte. The scan rate was 10 mV/s.

thin films and thus can be used for qualitative evaluation of the molecular packing of SAMs. Figure 1 shows the cyclic voltammograms (CVs) of EG<sub>6</sub>AC<sub>16</sub>H (a), EG<sub>6</sub>AC<sub>8</sub>H (b), and EG<sub>6</sub>AC<sub>2</sub>H (c) obtained in a 1.0 mM K<sub>3</sub>Fe(CN)<sub>6</sub> aqueous solution (also containing 100 mM KNO<sub>3</sub>). The low current density and the shape of the voltammograms confirm that the compounds form well-ordered SAMs with a small number of defects (pinholes). In all cases, the typical voltammetric waves from reduction/oxidation of the Fe(III)/Fe(II) species that are expected near the formal potential (0.2 V vs Ag/AgCl) are imperceptible. Hence, the majority of the faradaic current most likely stems from charge transfer via tunneling of electrons at packing disorders in the SAM.<sup>34</sup> This is also supported by the low hysteresis in the voltammograms, as well as the quasi-exponentially increasing cathodic current at more negative overpotentials. Another observation is that the longer the alkyl chains, the better the blocking capacity. This can be attributed to a more favorable molecular packing of the extended chain. Thus, the lack of a dense extended chain in the EG<sub>6</sub>AC<sub>2</sub>H SAM allows the redox species to penetrate the monolayer partially and reduces the overpotential for charge transfer. As expected, the EG<sub>6</sub>AC<sub>16</sub>H SAM provides the best blocking characteristics, but the improvement compared to EG<sub>6</sub>AC<sub>8</sub>H is smaller as compared to the improvement seen when going from two to eight carbons in the extended chain. These findings are in line with the contact angle and ellipsometric data, which suggested essentially the same molecular packing/orientation of the EG<sub>6</sub>AC<sub>8</sub>H and EG<sub>6</sub>AC<sub>16</sub>H SAMs. For comparison, also shown in Figure 1 is the CV of a hexadecanethiol SAM (d). The waviness in the CV near the formal potential and the increased current density clearly suggest a reduced blocking capacity for this SAM with respect to those analyzed in this study (a–c).

(34) Finklea, H. O. Electrochemistry of Organized Monolayers of Thiols and Related Molecules on Electrodes. In *Electroanalytical Chemistry: A Series of Advances*; Dekker: New York, 1996; Vol. 19, pp 109–335.

**3.3. Infrared Reflection Absorption Spectroscopy.** The majority of the bands in the RA spectra represented in Figure 2 can be easily identified by comparison with previous studies of related compounds.<sup>35–38</sup> The RA spectra of the EG<sub>6</sub>H and EG<sub>6</sub>AC<sub>16</sub>H SAMs have been reported by Valiokas et al.<sup>25,37</sup> All SAMs investigated in the present study were modeled by DFT calculations to understand the nature of related bands and to provide a quantitative or at least semiquantitative description of the spectral features. Table 3 lists the most distinctive bands seen in the RA spectra and their assignments. Some of the assignments are taken from previous extensive studies that are cited in Table 3.

**3.3.1. C–H Stretching Region.** As shown in Figure 2a, there are four vibrational modes arising from saturated hydrocarbons in the 3000–2800 cm<sup>-1</sup> region. Two of them are associated with methylene groups, and the other two are associated with terminal methyl group vibrations. This high-frequency region also contains oxyethylene stretching modes that are typical for ethylene glycols. In SAMs, this region provides important information about the molecular packing and the crystallinity of both the alkyl and ethylene glycol segments. In this particular series, the asymmetric methylene C–H stretching mode (d<sup>-</sup>) and the corresponding symmetric mode (d<sup>+</sup>) of the two alkyl segments are found at 2918 and 2850 cm<sup>-1</sup>, respectively. These positions are characteristic of densely packed and highly ordered alkyl chains adopting the all-trans conformation.

In the frequency region > 2930 cm<sup>-1</sup>, the first new feature, as compared to the EG<sub>6</sub>H reference spectrum, appears as a well-resolved band at 2938 cm<sup>-1</sup> in the EG<sub>6</sub>AC<sub>2</sub>H spectrum and as a shoulder for SAMs with longer alkyl chains. It is noteworthy that this feature is absent in the EG<sub>6</sub>AC<sub>1</sub>H spectrum, indicating that the nature of the band is related to the attachment of a methylene chain to the upper amide nitrogen. On the basis of the DFT calculations, we assign the band (or shoulder) at 2938 cm<sup>-1</sup> to a specific mode of the CH<sub>2</sub> symmetric stretching vibrations (d<sub>loc</sub><sup>+</sup>), which is strongly localized at the methylene group, the nearest neighbor to the upper amide. Further support of such an assignment is given by the fact that this is the dominating band in the EG<sub>6</sub>AC<sub>2</sub>H – EG<sub>6</sub>AC<sub>2</sub>D difference spectrum displayed in Figure 3. This observation agrees very well with the calculated TDMs, the largest of which corresponds to the localized d<sub>loc</sub><sup>+</sup> mode. In the Supporting Information, we present several examples of well-defined SAMs (e.g., ω-substituted alkanethiols on gold) where this mode appears whenever the SAM contains alkyl chains terminated by a methyl group on one end and a heteroatom on the other.

In contrast to the band discussed above, the features at higher frequencies demonstrate a rather complex dependence with increasing length of the upper alkyl chain; see Figure 2. In Table 3, these bands at 2947, 2956, 2963, 2965, and 2974 cm<sup>-1</sup> are all assigned to asymmetric CH<sub>3</sub> stretching vibrations. It is known from room-temperature RA spectra of well ordered *n*-alkanethiol SAM that the CH<sub>3</sub> asymmetric stretching vibrations appear as a single band at ~2964 cm<sup>-1</sup>.<sup>35</sup> At low temperatures, however, this band splits into a doublet and is assigned to out-of-plane (op ~2957 cm<sup>-1</sup>) and in-plane (ip ~2965 cm<sup>-1</sup>)

(35) Laibinis, P. E.; Whitesides, G. M.; Allara, D. L.; Tao, Y. T.; Parikh, A. N.; Nuzzo, R. G. *J. Am. Chem. Soc.* **1991**, *113*, 7152–7167.

(36) Vanderah, D. J.; Meuse, C. W.; Silin, V.; Plant, A. L. *Langmuir* **1998**, *14*, 6916–6923.

(37) Valiokas, R.; Svedhem, S.; Ostblom, M.; Svensson, S. C. T.; Liedberg, B. *J. Phys. Chem. B* **2001**, *105*, 5459–5469.

(38) Vanderah, D. J.; Arsenault, J.; La, H.; Gates, R. S.; Silin, V.; Meuse, C. W.; Valincius, G. *Langmuir* **2003**, *19*, 3752–3756.

(39) Valiokas, R.; Ostblom, M.; Svedhem, S.; Svensson, S. C. T.; Liedberg, B. *J. Phys. Chem. B* **2000**, *104*, 7565–7569.

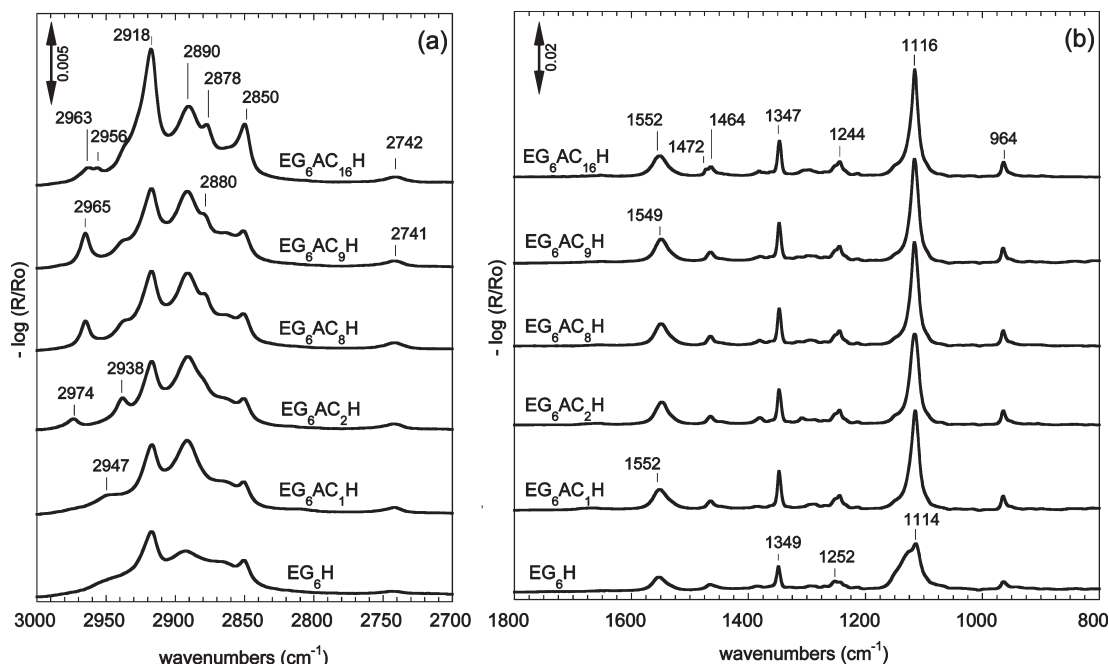


**Figure 2.** Infrared RA spectra of extended-chain alkanethiol SAMs. (a) CH-stretching region. (b) Fingerprint and amide regions.

**Table 3.** Band Assignments for Investigated Compounds EG<sub>6</sub>H and EG<sub>6</sub>AC<sub>*n*+1</sub>H with *n* = 0, 1, 7, 8, 15<sup>a</sup>

EG <sub>6</sub> H	EG <sub>6</sub> AC <sub>1</sub> H	EG <sub>6</sub> AC <sub>2</sub> H	EG <sub>6</sub> AC <sub>8</sub> H	EG <sub>6</sub> AC <sub>9</sub> H	EG <sub>6</sub> AC <sub>16</sub> H	assignment
964	965	964	965	965	964	CH <sub>2</sub> rocking and asym. COC stretching
1114	1115	1116	1116	1116	1116	asym. COC stretching
1252	1244	1244	1244	1244	1244	OEG CH <sub>2</sub> twisting
1349	1348	1348	1347	1347	1347	OEG CH <sub>2</sub> wagging
1466	1465	1465	1465	1465	1464/1472	OEG CH <sub>2</sub> bending
1553	1552	1548	1549	1549	1552	amide II
2744	2742	2743	2742	2742	2742	OEG CH <sub>2</sub> twisting + bending, combination
2851	2851	2851	2851 (2853)	2851	2850 (2851)	alkyl CH <sub>2</sub> sym. stretching (d <sup>+</sup> )
~2865	~2865	~2865	~2865	~2865	~2865	broad, OEG CH <sub>2</sub> sym. stretching
—	—	~2880	2880	2880	2878	sym. CH <sub>3</sub> stretching (r <sup>+</sup> )
2892	2891	2891	2891	2891	2890	OEG CH <sub>2</sub> asym. stretching
2917	2917	2917	2917 (2920)	2917	2918 (2917)	alkyl CH <sub>2</sub> asym. stretching (d <sup>-</sup> )
		2938	2938	2938	2938	alkyl CH <sub>2</sub> sym. stretching (d <sub>loc</sub> <sup>+</sup> )
	2947					asym. N-CH <sub>3</sub> out-of-plane stretching (r <sup>-</sup> op)
			2965	2965	2956	asym. CH <sub>3</sub> out-of-plane stretching (r <sup>-</sup> op)
			2965	2965	2963	asym. CH <sub>3</sub> in-plane stretching (r <sup>-</sup> ip)

<sup>a</sup> The assignments are in part based on previous work from our group<sup>28,29,32,39</sup> and on new calculations. Band frequencies (in cm<sup>-1</sup>) are also indicated in Figures 2 and 3. The spectral positions given in parentheses are obtained for the d<sup>+</sup> and d<sup>-</sup> bands of the extended chain (Figure 3).

stretching vibrations, respectively.<sup>26</sup> Thus, the measured spectra, represented in Figure 2, confirm the observations made before for ordered, room-temperature, *n*-alkanethiol SAMs on gold. The splitting observed for the EG<sub>6</sub>AC<sub>16</sub>H SAM into two components at 2956/2963 cm<sup>-1</sup>, however, is seldom observed at room temperature and is undoubtedly attributed to exceptionally well ordered extended methylene chains with a conformationally “locked” (or rotationally hindered) methyl group.<sup>25</sup> This is not more than a tentative explanation of the splitting effect that has a complex intra- and intermolecular nature<sup>40</sup> and deserves a separate and thorough investigation.

To elucidate the contribution of the extended chain, we have also generated RA spectra by subtracting the spectrum from the deuterated analogs of the same chain length from those in Figure 2. This can be done because the two sets of SAMs display virtually identical spectra in the fingerprint region; see section

3.3.4. Thus, the conformation and orientation of the constant portion appear to be independent of the nature of the tail group (D or H). The results after such a pairwise subtraction are shown in Figure 3.

Further on, we have performed a series of calculations to clarify the origins of the high-frequency bands in the RA spectra. Our DFT modeling shows that for the EG<sub>6</sub>AC<sub>1</sub>H molecule the TDM components of the CH<sub>3</sub> ip vibrations are an order of magnitude smaller than those of the op vibrations. This is a unique property of the CH<sub>3</sub> group directly attached to an amide moiety, which explains our assignment of the band at ~2947 cm<sup>-1</sup> to op CH<sub>3</sub> asymmetric vibrations. The spectral position of this band also agrees with the frequency range (2952–2942 cm<sup>-1</sup>) reported for *N*-methylformamide and its deuterated analogs.<sup>41</sup> Thus, we believe that the ip band is not observed because the corresponding TDM is too small.

(40) MacPhail, R. A.; Snyder, R. G.; Strauss, H. L. *J. Chem. Phys.* **1982**, *77*, 1118–1137.

(41) Suzuki, I. *Bull. Chem. Soc. Jpn.* **1962**, *35*, 540–551.

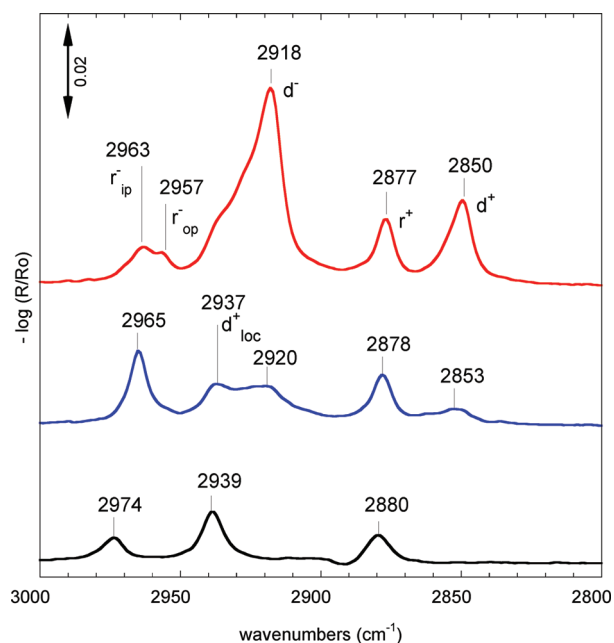


**Figure 3.** Infrared RA difference spectra are obtained by pairwise subtraction:  $\text{EG}_6\text{AC}_{n+1}\text{H} - \text{EG}_6\text{AC}_{n+1}\text{D}$ ,  $n = 1$  (black),  $n = 7$  (blue), and  $n = 15$  (red) to reveal the bands of the extended chains in the CH stretching region.

Similar calculations for  $\text{EG}_6\text{AC}_2\text{H}$  molecules show that the frequencies of op and ip vibrations change upon replacement of  $\text{C}_1\text{H}$  by  $\text{C}_2\text{H}$ . They are shifted upward and downward, respectively, and become closer to each other. The TDMs of op and ip vibrations are comparable, suggesting that the peak at  $2974\text{ cm}^{-1}$  in the  $\text{EG}_6\text{AC}_2\text{H}$  spectrum should be attributed to ip asymmetric vibrations. The red shift of this band from  $2974$  to  $2965\text{ cm}^{-1}$  in the RA spectra of the  $\text{EG}_6\text{AC}_8\text{H}$  and  $\text{EG}_6\text{AC}_9\text{H}$  SAMs is in very good agreement with the modeling results. These calculations show that for the large separation of the methyl group from the nitrogen atom, as in  $\text{C}_8\text{H}$  and  $\text{C}_9\text{H}$  chains, the frequencies of ip and op vibrations and the respective mode intensities are close to each other in their values. Therefore, it is most likely that the band at  $2965\text{ cm}^{-1}$  in the spectra of both SAMs represents contributions from both in-plane and out-of-plane  $\text{CH}_3$  asymmetric stretching vibrations, which are not resolved in the measured spectra.

A  $\text{CH}_3$  band at  $\sim 2880\text{ cm}^{-1}$ , which corresponds to the C–H symmetric stretching vibrations ( $r^+$ ), appears in the spectra of  $\text{EG}_6\text{AC}_{n+1}\text{H}$  SAMs,  $n = 1, 7, 8, 15$  (Figures 2 and 3). This mode is strongly localized on the terminal methyl group, and its intensity is therefore practically independent of the extended alkyl chain length, in contrast to the pronounced length dependence of the intensity of truly delocalized vibrations such as those resulting in the  $\text{CH}_2$  symmetric stretching band ( $d^+$ ) at  $\sim 2850\text{ cm}^{-1}$ . This feature is clearly seen if one compares the relative intensities of the  $r^+$  and  $d^+$  bands for the three spectra in Figure 3. The  $r^+$  band appears as a distinct band in all spectra, whereas the  $d^+$  band varies considerably in intensity with chain length. The same observation follows from our DFT calculations (data not shown). It is also evident in Figure 3 that  $d^+$  and  $d^-$  bands move upward a few wavenumbers to  $2853$  and  $2920\text{ cm}^{-1}$ , respectively, in the SAM of the  $\text{EG}_6\text{AC}_8\text{H}$  (and also for the  $\text{EG}_6\text{AC}_9\text{H}$  SAM), which is indicative of a slight disordering of the alkyl chains of this length.

The relative intensities of methyl asymmetric ( $r^-$ ) to symmetric stretches ( $r^+$ ) are well known to follow an odd–even chain length effect<sup>42</sup> as a result of different orientations of their TDMs with respect to the gold surface. The intensity of the  $r^+$  band is normally larger than that of the  $r^-$  band in SAMs with an odd number of methylene groups in the chain and smaller for even-numbered chains.<sup>43</sup> The  $\text{EG}_6\text{AC}_8\text{H}$  (odd  $\text{CH}_2$ ) SAM has a larger relative intensity  $r^+/r^-$  ratio than does the  $\text{EG}_6\text{AC}_9\text{H}$  (even  $\text{CH}_2$ ) SAM (Supporting Information). This observation agrees very well with earlier reports. For long-chain  $\text{EG}_6\text{AC}_{16}\text{H}$ , we do not have access to SAMs with an even number of alkyl chains in the extended chain.

The OEG segment possesses a strong absorption band near  $2890\text{ cm}^{-1}$ , previously assigned to the symmetric stretching mode.<sup>44</sup> It was recently reassigned by Malysheva et al. to the asymmetric methylene stretching vibrations.<sup>28,30</sup> This band is characteristic of the helical OEG conformation and is independent of the extended alkyl chain length. It is well resolved in all SAMs with two amide groups but nearly washed away in  $\text{EG}_6\text{H}$  SAMs. This drastic change is accompanied, as seen in Figure 2, by a concomitant decrease in intensity and by broadening of the COC stretching band, which, in addition, acquires pronounced asymmetry. It was pointed out that the asymmetry of the broad COC stretching band in the  $\text{EG}_6\text{H}$  spectrum can be explained by the presence of  $\sim 10\%$  defects in the form of intact OEG chains adopting the all-trans conformation.<sup>32</sup> The same type of defect can very well explain the decrease in intensity and broadening of the band of OEG  $\text{CH}_2$  asymmetric stretching vibrations as compared to those for the SAMs containing the extended alkyl chains. The corresponding symmetric OEG methylene stretching band is not seen because of strong overlapping with other bands. Another characteristic absorption of the helical OEG chain is the weak band at  $\sim 2742\text{ cm}^{-1}$  that is assigned to a combination band of  $\text{CH}_2$  twisting and scissoring modes.<sup>30,44</sup>

**3.3.2. Fingerprint Region: OEG Contribution.** The low-frequency region,  $1800\text{--}800\text{ cm}^{-1}$ , is primarily used for the characterization of the conformational characteristics of the OEG and amide portions. The alkyl bands are generally much less intense and hardly resolved for the present set of SAMs. As shown in Figure 2b, the fingerprint region of the helical OEG segment in the series consists of a  $\text{CH}_2$  scissoring mode that originates from both the alkyl and OEG chains at  $1465\text{ cm}^{-1}$ , a sharp  $\text{CH}_2$  wagging at  $1347\text{ cm}^{-1}$ , a weak  $\text{CH}_2$  twisting band mainly at  $1244\text{ cm}^{-1}$ , and a combination band of methylene C–H rocking and COC stretching at  $964\text{ cm}^{-1}$ . These  $1347$ ,  $1244$ , and  $964\text{ cm}^{-1}$  bands are all very characteristic of the helical conformation, and they are seen in the IR spectra of crystalline PEG.<sup>44</sup> Except for the  $\text{EG}_6\text{H}$  SAM, a strong, sharp feature is also seen at  $1116\text{ cm}^{-1}$ , and it is attributed to the asymmetric C–O–C stretching vibration (Table 3). It has a weak shoulder on the high-frequency side that has been attributed to the multimode nature of the C–O–C stretching vibration, and it is a typical feature of a helical phase.<sup>30</sup> These vibrations are associated with TDMs aligned along the helical axis. Their intensity and sharpness (which in turn indicates structural uniformity) suggest that the helical axis for the entire series is oriented similarly as in the  $\text{EG}_6\text{H}$  SAM regardless of the extended chain length.<sup>29</sup> It is interesting that the RA spectra for the  $\text{EG}_6\text{AC}_{1-16}\text{H}$  series are virtually identical in the  $1800\text{--}800\text{ cm}^{-1}$  region, suggesting that the constant portion of the constituting molecules is structurally

(43) Nishi, N.; Hobara, D.; Yamamoto, M.; Kakiuchi, T. *J. Chem. Phys.* **2003**, *118*, 1904–1911.

(44) Miyazawa, T.; Fukushima, K.; Ideguchi, Y. *J. Chem. Phys.* **1962**, *37*, 2764–2776.

(42) Tao, F.; Bernasek, S. L. *Chem. Rev.* **2007**, *107*, 1408–1453.

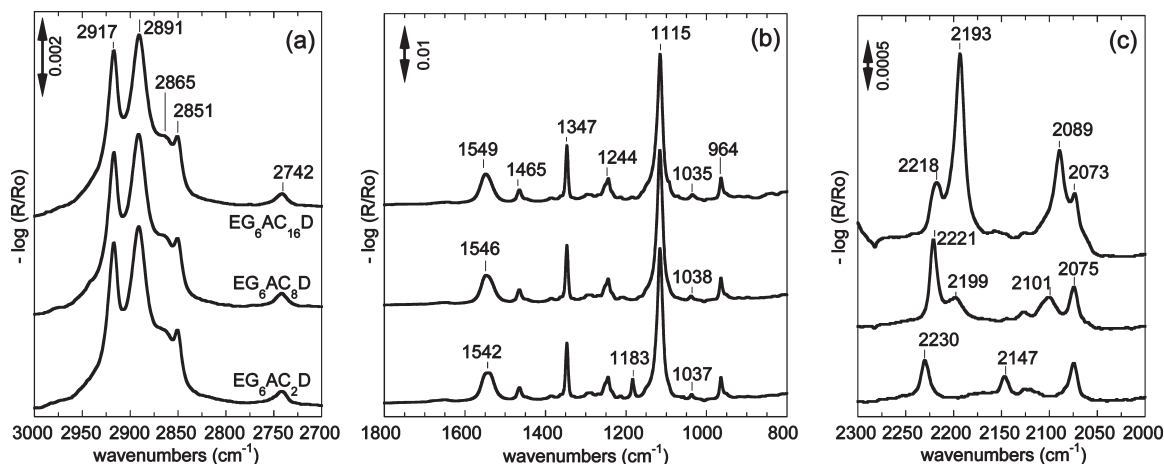


**Figure 4.** Infrared RA spectra of deuterated extended-chain OEG alkylthiol SAMs. (a) CH stretching region. (b) Fingerprint and amide regions. (c) CD stretching region.

identical in all SAMs investigated in this study. The only visible difference is the doublet at  $1464/1472\text{ cm}^{-1}$  in the  $\text{EG}_6\text{AC}_{16}\text{H}$  SAM, which originates from a superposition of  $\text{CH}_2$  scissoring vibrations from the highly organized extended chain ( $1472\text{ cm}^{-1}$ ) and from the OEG and alkylthiol chains ( $1465\text{ cm}^{-1}$ ).

The RA spectrum of the  $\text{EG}_6\text{H}$  SAM differs from those discussed above. The helical bands decrease in intensity and shift a few wavenumbers. The most prominent change is seen for the main band at  $1114\text{ cm}^{-1}$ , which contains shoulders at around  $1126$  and  $1150\text{ cm}^{-1}$ . These shoulders have been previously attributed to the coexistence of several different OEG phases in the SAM (amorphous and all-trans).<sup>22,23</sup> Recent theoretical work from our group suggests that the amide group of this particular class of amide-bridged OEG SAMs contributes to the appearance of a shoulder on the high-frequency side of the main band. However, the main reason for its broadness and strong asymmetry was attributed to the coexistence of a small percentage of  $\text{EG}_6\text{H}$  molecules in the all-trans conformation (defects) in a background of molecules with helical chains.<sup>32</sup> This factor is largely excluded in SAMs containing the second amide bridge that apparently prevents the coexistence of two OEG conformers, making the COC peak more intense and nearly symmetric.<sup>27</sup>

**3.3.3. Fingerprint Region: Amide Contribution.** The two amide linkages introduced between the alkyl and OEG portions create lateral hydrogen bonding networks within the SAM, which contribute to the favorable packing of the alkyl chains and improved SAM stability.<sup>14,29,37</sup> In Figure 2b, the band at  $1552\text{ cm}^{-1}$  is assigned to the amide II vibration and shifts to lower frequency, indicating that in-plane hydrogen bonding weakens in the SAMs with shorter extended chains.<sup>14,45</sup> The appearance of an intense amide II band and an extremely weak amide I band (expected to appear at  $\sim 1650\text{ cm}^{-1}$ ) suggests that both amides are highly oriented with respect to the metal surface with the C=O bond nearly perpendicular to the surface normal.<sup>46</sup> The intensities and widths of the amide II band vary slightly depending on the extended alkyl chain lengths, suggesting that the two amide linkages are not identical. Most likely, the first amide group has a fixed orientation as a result of the long, well-ordered alkylthiol chain and helical OEG segment, whereas the hydrogen bonding of the second amide linkage appears to be dependent on the length of the extended alkyl chain.

**3.3.4. Mode Assignments of Deuterated Extended-Chain OEG Alkylthiol SAMs.** The RA spectra of the  $\text{EG}_6\text{AC}_{n+1}\text{D}$  SAMs,  $n = 1, 7,$  and  $15,$  are shown in Figure 4, and the mode assignments obtained from the DFT calculations are given in Table 4. As displayed in Figure 4a, the relative intensities of the  $d^-$  and  $d^+$  bands at  $2917$  and  $2851\text{ cm}^{-1}$ , respectively, as well as the characteristic bands of the OEG portion at  $2891$  and  $2742\text{ cm}^{-1}$  are identical regardless of the extended-chain length. These band positions are again characteristic of densely packed and highly ordered all-trans alkyl chains and a helical OEG phase, respectively. The frequencies and relative intensities of the bands associated with vibrations of the constant portion of the molecules within the three SAMs displayed in the fingerprint region (Figure 4b) agree with those of the nondeuterated compounds in Figure 2b. Thus, there is no doubt that the constant portion of the molecules in the SAMs adopts an identical structure regardless of whether we are using deuterated or nondeuterated extended chains of varying length.

Figure 4c shows the vibrations of the deuterated chain in the C–D stretching region between  $2300$  and  $1900\text{ cm}^{-1}$ . The RA spectrum of the  $\text{EG}_6\text{AC}_{16}\text{D}$  SAM exhibits two strong methylene C–D stretching modes at  $2193\text{ cm}^{-1}$  (asymmetric,  $d^-$ ) and  $2089\text{ cm}^{-1}$  (symmetric,  $d^+$ ), respectively. These peaks are assigned to extended chains adopting a highly ordered all-trans conformation. For the  $\text{EG}_6\text{AC}_8\text{D}$  SAM, both bands shift to higher frequencies and appear at  $2199$  and  $2101\text{ cm}^{-1}$ , respectively, and their intensities decrease dramatically. This behavior is in line with the findings for the alkyl chain of the nondeuterated compounds of the same length (Figure 3) and suggests a slight disordering of the extended chain. Methyl C–D vibrations appear at  $2218\text{ cm}^{-1}$  ( $r^-$ ) and  $2073\text{ cm}^{-1}$  ( $r^+$ ) for the  $\text{EG}_6\text{AC}_{16}\text{D}$  SAM. The trends in terms of intensity changes and frequency shifts upon decreasing the length of the extended chain are again virtually identical to those observed for the nondeuterated analogs in Figure 3.

Surprisingly, the amide II frequency undergoes a red shift that increases with the length of the deuterated alkyl chain. This effect is fully reproduced in the DFT calculations as shown in Table 5. The observed red shift of the amide II band has an intramolecular nature and can be attributed to an increased effective mass of the nitrogen atom coupled with a heavier deuterated alkyl.

An interesting and unexpected manifestation of the red shift concerns amide III vibrations that do not show up directly in the observed spectra. Commonly, these vibrations are understood as collective N–H in-plane bending and C–N stretching motions

(45) Clegg, R. S.; Hutchison, J. E. *Langmuir* **1996**, *12*, 5239–5243.

(46) Valiokas, R.; Svedhem, S.; Svensson, S. C. T.; Liedberg, B. *Langmuir* **1999**, *15*, 3390–3394.

**Table 4. Band Assignments for Investigated Compounds EG<sub>6</sub>AC<sub>n+1</sub>D, n = 1, 7, 15<sup>a</sup>**

EG <sub>6</sub> AC <sub>2</sub> D	EG <sub>6</sub> AC <sub>8</sub> D	EG <sub>6</sub> AC <sub>16</sub> D	assignment
965	965	964	CH <sub>2</sub> rocking and asym. COC stretching
1037	1038	1035	CD <sub>2</sub> and CD <sub>3</sub> bending
1116	1116	1115	asym. COC stretching
1183		1184, weak	CD <sub>2</sub> wagging coupled with amide III and CH <sub>2</sub> wagging coupled with amide III
1245	1245	1244	OEG CH <sub>2</sub> twisting
1347	1347	1347	OEG CH <sub>2</sub> wagging
1465	1465	1465	OEG CH <sub>2</sub> bending
1542	1546	1549	amide II
2075	2075	2073	CD <sub>3</sub> sym. stretching (r <sup>+</sup> )
	2101	2089	CD <sub>2</sub> sym. stretching (d <sup>+</sup> )
2147	2145	~2155, weak	CD <sub>2</sub> sym. stretching (d <sup>+</sup> loc)
	2199	2193	CD <sub>2</sub> asym. stretching (d <sup>-</sup> )
2230			CD <sub>3</sub> asym. stretching (r <sup>-</sup> op)
	2221	2218	CD <sub>3</sub> asym. stretching (r <sup>-</sup> ip)
2742	2742	2742	OEG CH <sub>2</sub> twisting + bending, combination
2851	2851	2851	alkyl CH <sub>2</sub> sym. stretching (d <sup>+</sup> )
~2865	~2865	~2865	broad, OEG CH <sub>2</sub> sym. stretching
2891	2891	2891	OEG CH <sub>2</sub> asym. stretching
2917	2917	2917	alkyl CH <sub>2</sub> asym. stretching (d <sup>-</sup> )

<sup>a</sup> Band frequencies are in cm<sup>-1</sup>.

**Table 5. Calculated Frequencies (Scaling Factor of 1.032), TDM Components, And Integral Intensity of C–N1 and C–N2<sup>a</sup> Vibrations That Form the Amide II Band<sup>b</sup>**

molecule	frequency (cm <sup>-1</sup> )	TDMx	TDMy	TDMz	intensity	assignment
EG <sub>6</sub> AC <sub>16</sub> H	1548	0.2	-3.5	13.2	13.7	C–N1
	1554	2.8	-4.4	12.9	13.9	C–N2
EG <sub>6</sub> AC <sub>16</sub> D	1548	0.1	-3.4	12.9	13.3	C–N1
	1536	3.5	-5.0	14.6	15.8	C–N2

<sup>a</sup> N1 (N2) refers to the lower (upper) amide. <sup>b</sup> Similar calculations for molecules with shorter deuterated alkyl chains exhibit the same trend.

with characteristic frequencies of ~1200 cm<sup>-1</sup>. In our previous related reports<sup>38</sup> as well as in the present study of nondeuterated SAMs, no unambiguous signatures of these vibrations were observed. To our knowledge, the amide III vibrations have never been recorded in SAMs stabilized by a lateral hydrogen bonding network of amide moieties.<sup>45,47</sup> However, in the EG<sub>6</sub>AC<sub>2</sub>D RA SAM spectrum, these vibrations become visible as described below.

Besides the above-mentioned N–H and C–N coupled vibrations, there are combined CN–CH<sub>2</sub> vibrations at ~1177 cm<sup>-1</sup> that involve the CH<sub>2</sub> wagging motions of the lower-part alkyls and C–N stretching motions of CONH1 and vibrations at ~1200 cm<sup>-1</sup> that involve similar motions of the upper-part alkyls and CONH2. The frequency of the latter vibration is calculated to be 1173 cm<sup>-1</sup> for EG<sub>6</sub>AC<sub>2</sub>D, 1161 cm<sup>-1</sup> for EG<sub>6</sub>AC<sub>8</sub>D, and 1155 cm<sup>-1</sup> for EG<sub>6</sub>AC<sub>16</sub>D, whereas the 1177 cm<sup>-1</sup> frequency remains unchanged. The accidental near-coincidence of CONH1 and CONH2 vibrational frequencies for EG<sub>6</sub>AC<sub>2</sub>D nearly doubles the apparent intensity of the respective amide III band. Thus, the peak at 1183 cm<sup>-1</sup> that appears only in the spectrum of the EG<sub>6</sub>AC<sub>2</sub>D SAM can be understood as two overlapping bands, one associated with CH<sub>2</sub> wagging vibrations of the alkyls coupled with C–N1 stretching vibrations and the other associated with CD<sub>2</sub> wagging vibrations of deuterated alkyls coupled with C–N2 stretching vibrations.

To summarize, the data reveal a small amount of disorder in extended chains of intermediate length by analogy to the observations for the corresponding nondeuterated compounds. The shifts of the amide II bands for the deuterated compounds are

also very interesting and may have implications for the extended chain organization. This will be further discussed in the following sections.

### 3.4. Model Results on Molecular Orientation and Infrared RA Spectra.

**3.4.1. Optimized Molecular Geometry.** Calculations of optimized molecular geometries, vibrational spectra, and transition dipole moments (TDMs) of molecules EG<sub>6</sub>AC<sub>n+1</sub>H with n = 0, 1, 7, 8, and 15 were performed by using the DFT BP86 method with a 6-31G\* basis set. First, these data were used to assign new features in the RA spectra that appeared as a result of an additional, amide-coupled alkyl layer on top of the supporting EG<sub>6</sub>H SAM. The corresponding results have been discussed in the preceding sections. Here, the focus is primarily on the molecular orientation within the SAMs, which is of crucial importance in understanding the volume and surface properties of these, in many respects new, systems.

The DFT calculations predict that two conformers of the molecular series EG<sub>6</sub>AC<sub>n+1</sub>H exhibit equilibrium geometries consistent with an extended self-assembled architecture. These conformers labeled as I and II, which differ from each other by the dihedral τ<sub>2</sub>(CNCC) of the upper amide group, negative ≈ -100° for I and positive ≈ 110° for II, are shown in Figure 5. The supporting alkyl chain C<sub>15</sub> has the same orientation for all molecules. The difference in orientation of the molecular components reflects the dependence of the Euler angles of OEG and both amide groups on the conformational state and also on the length of the extended chain. Importantly, in this variety of molecular forms, the orientation of the O–C–N skeleton of both amide groups remains favorable for the formation of two hydrogen bonding networks parallel to the substrate. Moreover, the equilibrium energies of conformers I and II are practically equal.

Our calculations also show that the optimized geometry of the lower portion does not change much and remains similar to the equilibrium geometry of molecule EG<sub>6</sub>H. In contrast, the values of ∠(z<sub>C<sub>15</sub></sub>, z<sub>C<sub>n</sub>H</sub>), the angle between the molecular axes of the lower and upper alkyls, vary quite appreciably, up to 20°. Furthermore, in conformer I, the upper alkyl chain tends to continue in the direction of the lower alkyl chain, whereas z<sub>C<sub>15</sub></sub> and z<sub>C<sub>n</sub>H</sub> axes of conformer II are tilted in almost opposite directions. This suggests that the presence of a considerable number of conformer II species in SAMs built from conformer I species would substantially deteriorate the SAM structural homogeneity, leading to readily detected band distortions in the CH region of the RA spectrum.

(47) Clegg, R. S.; Hutchison, J. E. *J. Am. Chem. Soc.* **1999**, *121*, 5319–5327.

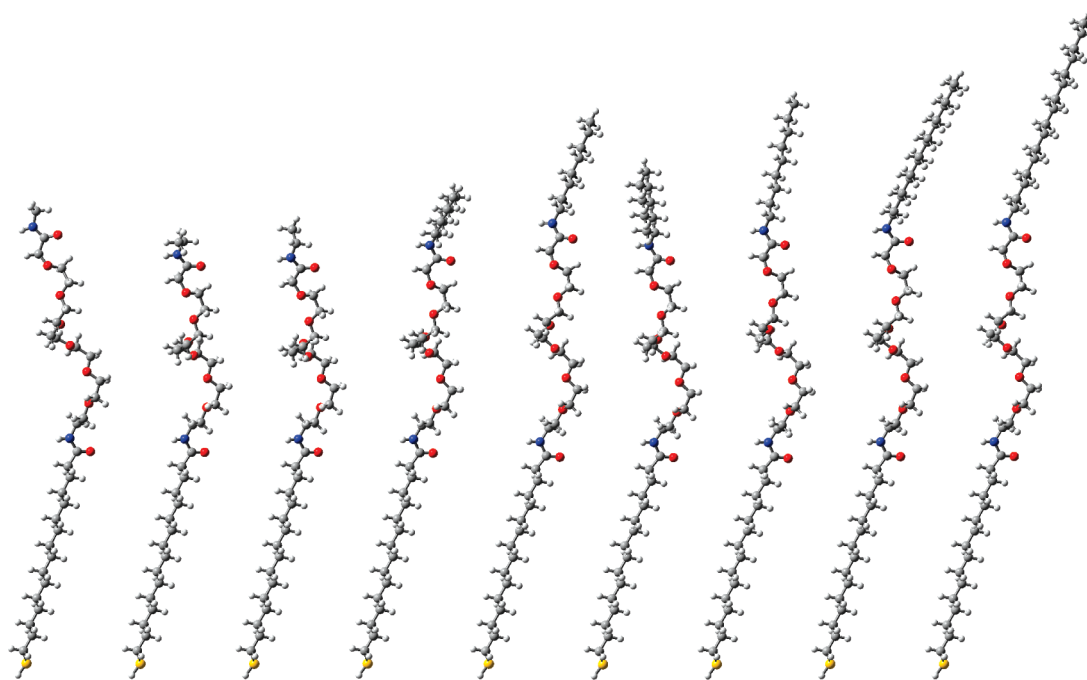


**Figure 5.** (Left to right) EG<sub>6</sub>AC<sub>1</sub>H molecule (one conformer) and pairs of conformers I and II of EG<sub>6</sub>AC<sub>*n*+1</sub>H, *n* = 1, 7, 8, 15.

**Table 6. Best-Fit Angles of Molecular Orientation within Model Self-Assemblies EG<sub>6</sub>H and EG<sub>6</sub>AC<sub>*n*+1</sub>H<sup>a</sup>**

molecule	$\theta_{CnH}$	$\psi_{C15}$	$\theta_{CnH}$	$\theta_E$	$\gamma_{c1=O1}$	$\gamma_{c2=O2}$
EG <sub>6</sub> H		−60°		22°	93°	
EG <sub>6</sub> AC <sub>1</sub> H	32°	−60°		31°	88°	74°
EG <sub>6</sub> AC <sub>2</sub> H	48°/26°	−110°/−110°		24°/26°	103°/103°	94°/92°
EG <sub>6</sub> AC <sub>8</sub> H	40°/33°	−110°/−70°	129°/227°	20°/25°	107°/97°	97°/93°
EG <sub>6</sub> AC <sub>9</sub> H	40°/17°	−110°/−60°	129°/229°	20°/29°	107°/95°	97°/90°
EG <sub>6</sub> AC <sub>16</sub> H	39°/36°	−110°/−70°	117°/222°	15°/25°	106°/96°	98°/94°

<sup>a</sup> The data is presented for conformers I/II, *n* = 0, 1, 7, 8, 15, and is calculated for the fixed tilt angle  $\theta_{C_{15}} = 20^\circ$  and variable rotation angle  $\psi_{C_{15}}$  of the lower alkyl C<sub>15</sub>.  $\theta_{CnH}$  and  $\psi_{CnH}$  are the tilt and rotational angles of the upper alkyl CCC plane,  $\theta_E$  is the OEG tilt angle, and  $\gamma_{c1=O1}$  and  $\gamma_{c2=O2}$  are angles between the substrate normal and C=O bond of the lower and upper amide, respectively.

Such distortions are not seen, suggesting that a mixed type of assembly composed of conformers I and II is very unlikely.

**3.4.2. In-SAM Molecular Orientation.** To be able to draw conclusions about the in-SAM molecular orientation, we have performed large-scale ab initio modeling, the principal steps of which are described in ref 29. The essence of our strategy is to find tilt ( $\theta_{C_{15}}$ ) and rotational ( $\psi_{C_{15}}$ ) angles of the basic alkyl C<sub>15</sub> that are consistent with experimentally observed intensities of symmetric and asymmetric bands in the CH stretching region to ensure that angles  $\gamma_{c1=O1}$  and  $\gamma_{c2=O2}$  between amide C=O bonds of both amide groups and the SAM surface normal are close to 90° and to reach an agreement between the calculated and measured SAM thicknesses, as shown in Table 2. Note that both conformers give similar thicknesses and display very small differences between the respective model RA spectra. According to this modeling,  $\theta_{C_{15}} \approx 20^\circ$  indicating the general tendency toward a smaller tilt of the lower alkyl in SAMs stabilized by two amides in comparison with EG<sub>6</sub>H SAMs, where  $\theta_{C_{15}} \approx 25^\circ$ .<sup>29</sup> The best-fit rotational angles  $\psi_{C_{15}}$  obtained at  $\theta_{C_{15}} = 20^\circ$  as well as the corresponding orientational angles for the OEG portion, both amides, and upper alkyls in newly studied SAMs are summarized in Table 6. These data show that in the (likely) in-SAM molecular orientation the OEG portion has a smaller tilt angle in conformation I as compared to that in conformation II. For example, in EG<sub>6</sub>AC<sub>16</sub>H-I,  $\theta_E \approx 15^\circ$ , which is the smallest calculated OEG tilt. This result can be considered to be a pro argument indicating that in studied SAMs

the lower and upper alkyl chains are preferably aligned to each other as they are in conformers having negative dihedral angle  $\tau_2(\text{CNCC})$ .

We have also examined the steric fitness of conformers I and II with different lengths of the upper alkyl for the formation of a double hydrogen-bonding network. It was found that all members of the family can form a 2D hexagonal structure on the Au(111) surface. Despite the substantial differences in the orientation of the extended chains having different lengths, the H···O distance turned out to be sufficiently small to enable the formation of hydrogen bonds. For free-standing molecules in the hexagonal arrangement, the calculated H···O distance falls in the range of 2.5–3 Å. As shown in recent ab initio calculations performed for related periodic arrays,<sup>31</sup> on the basis of such lengths, the initial geometry undergoes a significant adjustment of the molecules to the SAM environment and a concomitant reduction of the H···O length to a more reasonable value of ~1.9 Å. Thus, a plausible, though idealized, picture of EG<sub>6</sub>AC<sub>*n*+1</sub>H orientation may look like that in Figure 6.

**3.4.3. Model Infrared RA Spectra.** Under the assumption that the in-SAM molecular orientation is close to that specified in Table 6 and using the DFT-calculated TDMs of vibrational modes of molecules EG<sub>6</sub>AC<sub>*n*+1</sub>H, the RA spectra have been calculated according to the earlier suggested scheme.<sup>29</sup> Figure 7 represents typical spectra in the fingerprint region that model the measured spectra shown in Figure 2b. The frequencies and TDMs

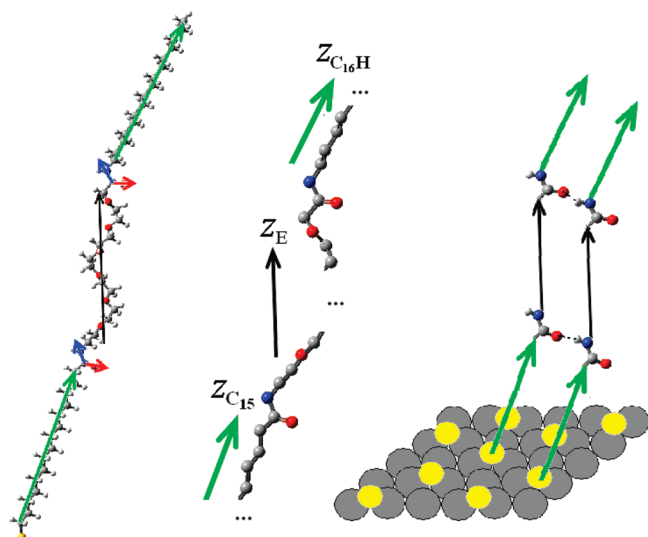


**Figure 6.** Real-space configuration of molecule  $\text{HS}-(\text{CH}_2)_{15}-\text{CONH}-(\text{CH}_2\text{CH}_2\text{O})_6-\text{CH}_2-\text{CONH}-(\text{CH}_2)_{15}-\text{CH}_3$  (left) and its more detailed representation in amide regions (middle), repeated by the molecular axes of alkyls  $\text{C}_{15}$ ,  $\text{C}_{16}\text{H}$  (green arrows), and OEG (black arrow). Conformer I optimized geometry is assumed. (Right) Possible formation of hydrogen bonds in  $\text{EG}_6\text{AC}_{16}\text{H}$  SAMs with sulfur atoms arranged in a hexagonal overlayer on the  $\text{Au}(111)$  surface.

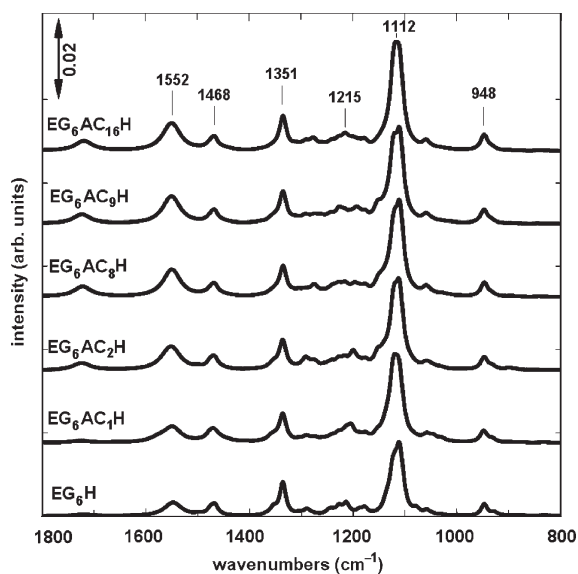


**Figure 7.** Infrared RA spectra of molecules  $\text{EG}_6\text{C}_{n+1}\text{H}$  as calculated by the BP86/6-31G\* method for conformer I oriented with respect to the substrate according to Table 6.  $\text{hwhm} = 8 \text{ cm}^{-1}$  for the fingerprint region and  $20 \text{ cm}^{-1}$  for amide peaks; the scaling factor is 1.032 for amide II peaks.

of the OEG portion were not scaled. The only scaling factor, 1.032, corrects the amide II peak. The  $\text{hwhm}$  indicated in the Figure caption was supposed to be constant and different for OEG and amide Lorentzian-shaped bands. This minimal set of fitting parameters and the use of optimal orientation angles represented in Table 6 provide impressive agreement between the model spectra in Figure 7 and experiment (Figure 2b). However, even qualitatively, the reproduction of measured spectra by modeling at the single-molecule level is not totally correct. This observation is worth discussing.

As observed in the experiment, adding an extra amide group nearly doubles the intensity of the amide II peak at  $\sim 1550 \text{ cm}^{-1}$

but has no visible effect on the amide I band, which is very weak in all measured spectra (Figure 2b). This is in contrast to the model spectra, where the amide I band is absent only in  $\text{EG}_6\text{H}$  and  $\text{EG}_6\text{AC}_1\text{H}$  spectra. It appears, however, as a well-resolved feature at  $\sim 1700 \text{ cm}^{-1}$  in the model RA spectra of molecules  $\text{EG}_6\text{AC}_{n+1}\text{H}$ ,  $n = 1, 7, 8,$  and  $15$  (Figure 7) because of the reorientation of the OCN plane. We propose, therefore, that it is the formation of the second layer of hydrogen bonding  $\text{NH}\cdots\text{O}=\text{C}$  between the nearest-neighbor molecules that keeps TDM of the  $\text{C}=\text{O}$  vibrations practically parallel to the substrate surface in all SAMs with extended chains.

Furthermore, the COC band is the dominating feature in both the experimental and calculated spectra. The multimode structure of this band is an inherent property of this type of SAM,<sup>30,32</sup> and the larger width of this band in the model spectra is attributed to contributions from several intense modes that are slightly shifted with respect one to another. Also, the shape of the measured COC band is much less affected by the length of the  $\text{C}_n\text{H}$  chain than predicted by modeling the free-molecule spectrum. A likely explanation of the divergence between theory and experiment is that in SAMs with an upper amide-bridged alkyl portion the intermolecular interaction leads to an intensity redistribution of the COC stretching modes, causing the one at  $1116 \text{ cm}^{-1}$  to dominate the others. In fact, this implies that SAMs with two networks of hydrogen bonding possess much better crystal structure than the basic  $\text{EG}_6\text{H}$  SAM, where the width of the COC band is inherently larger and additionally increased by the presence of all-trans OEG defects. No traces of such defects can be seen in SAMs with extended chains.

#### 4. Conclusions

We have presented an experimental and theoretical study on the assembly and structural characterization of a series of complex compounds composed of a constant portion of an  $n$ -alkylthiol linked to a hexa(ethylene glycol) module that is terminated with an  $n$ -alkyl chain of varying length. A few of the compounds were also synthesized with a deuterated extended chain, enabling us to address the structural characteristics of the supporting and extended  $n$ -alkyl chains selectively. The experimental data clearly points toward the formation of highly ordered and oriented assemblies regardless of the length of the extended chain, an observation that increases the interest in using the present set of SAMs as templates for the growth of more complicated and mixed architectures (e.g., supported lipid membrane formation). Extensive DFT calculations on the present series and on related compounds have provided an in depth understanding of the origin of almost all bands seen in experimental RA spectra and of the molecular orientation of the constituting molecules.

It is argued that  $\text{CH}_2$  symmetric vibrations of the alkyl chain are signified by two bands,  $\text{d}^+$  at  $\sim 2850 \text{ cm}^{-1}$  and  $\text{d}_{\text{loc}}^+$  at  $2938 \text{ cm}^{-1}$ . The former represents the normal (collective)  $\text{CH}_2$  vibrations, whereas the  $\text{d}_{\text{loc}}^+$  band is specific for  $N$ -terminated alkyl chains  $\cdots-\text{NH}-(\text{CH}_2)_n-\text{CH}_3$  and originates from vibrations that are strongly localized at the methylene group next to the heteroatom. This vibration is practically independent of alkyl length and explains the constant intensity and spectral position of the  $\text{d}_{\text{loc}}^+$  band. It is shown both experimentally and theoretically that alkyl deuteration results in a red shift of amide II characteristic frequencies. This shift is clearly recorded in the SAM series  $\text{EG}_6\text{AC}_{n+1}\text{D}$ ,  $n = 1, 7,$  and  $15$ . The same effect makes the amide III vibrations visible as a band at  $1183 \text{ cm}^{-1}$  in the  $\text{EG}_6\text{AC}_2\text{D}$  spectrum. The appearance of this band was assigned

to the accidental coincidence of the red-shifted and non-shifted amide III frequencies in deuterated and nondeuterated alkyl portions.

Extensive *ab initio* modeling has been performed to determine the orientation of molecules within studied SAMs. The likely tilt and rotational angles of basic alkyl are shown to be about  $20^\circ$  and  $-110^\circ$ , respectively. The suggested molecular orientation is in excellent agreement with the measured RA spectra in the fingerprint region and supports the formation of two in-plane stabilizing networks of hydrogen-bonded amides.

Pure and mixed monolayers of the compounds presented in this study are currently explored in conjunction with the formation of lipid mono- and multilayer architectures as well as in the

fabrication of hydrogel-based nanomaterials and will be reported elsewhere.

**Acknowledgment.** This work was supported by the Swedish Research Council (VR), the Swedish Institute (SI) through the Visby program, and the Lithuanian State Science and Studies Foundation.

**Supporting Information Available:** Transmission infrared spectra of the synthesized compounds. Odd–even effect in the CH stretching region of the SAM IR spectra. Calculation of  $d_{\text{loc}}^+$  for different SAMs. This material is available free of charge via the Internet at <http://pubs.acs.org>.